Geoscience Frontiers 10 (2019) 725–751

HOSTED BY

ELSEVIER

Contents lists available at ScienceDirect

China University of Geosciences (Beijing)

Geoscience Frontiers

journal homepage: www.elsevier.com/locate/gsf

Research Paper

Oligocene subduction-related plutonism in the Nodoushan area, Urumieh-Dokhtar magmatic belt: Petrogenetic constraints from U–Pb zircon geochronology and isotope geochemistry

Badieh Shahsavari Alavijeh [a], Nematollah Rashidnejad-Omran [a,*], Fatma Toksoy-Köksal [b], Wenliang Xu [c,d], Jalil Ghalamghash [e]

[a] Department of Geology, Faculty of Basic Sciences, Tarbiat Modares University, P.O. Box 14155–175, Tehran, Iran
[b] Department of Geological Engineering, Middle East Technical University, TR-06531, Ankara, Turkey
[c] College of Earth Sciences, Jilin University, Changchun 130061, China
[d] State Key Laboratory of Geological Processes and Mineral Resources, China University of Geosciences, Wuhan 430074, China
[e] Research Institute for Earth Sciences, Geological Survey of Iran, P.O. Box 13185–14194, Tehran, Iran

ARTICLE INFO

Article history:
Received 23 October 2017
Received in revised form
20 January 2018
Accepted 23 March 2018
Available online 25 May 2018
Handling Editor: Yener Eyuboglu

Keywords:
Urumieh–Dokhtar magmatic belt
Granitoid rocks
Subduction
Zircon U–Pb ages
Radiogenic isotopes
Central Iran

ABSTRACT

Geochemical data and Sr–Nd isotopes of the host rocks and magmatic microgranular enclaves (MMEs) collected from the Oligocene Nodoushan Plutonic Complex (NPC) in the central part of the Urumieh –Dokhtar Magmatic Belt (UDMB) were studied in order to better understand the magmatic and geodynamic evolution of the UDMB. New U–Pb zircon ages reveal that the NPC was assembled incrementally over ca. 5 m.y., during two main episodes at 30.52 ± 0.11 Ma and 30.06 ± 0.10 Ma in the early Oligocene (middle Rupelian) for dioritic and granite intrusives, and at 24.994 ± 0.037 Ma and 24.13 ± 0.19 Ma in the late Oligocene (latest Chattian) for granodioritic and diorite porphyry units, respectively. The spherical to ellipsoidal enclaves are composed of diorite to monzodiorite and minor gabbroic diorite (SiO_2 = 47.73–57.36 wt.%; Mg# = 42.15–53.04); the host intrusions are mainly granite, granodiorite and diorite porphyry (SiO_2 = 56.51–72.35 wt.%; Mg# = 26.29–50.86). All the samples used in this study have similar geochemical features, including enrichment in large ion lithophile elements (LILEs, e.g. Rb, Ba, Sr) and light rare earth elements (LREEs) relative to high field strength elements (HFSEs) and heavy rare earth elements (HREEs). These features, combined with a relative depletion in Nb, Ta, Ti and P, are characteristic of subduction-related magmas. Isotopic data for the host rocks display I_{Sr} = 0.705045–0.707959, $\varepsilon_{Nd}(t)$ = −3.23 to +3.80, and the Nd model ages (T_{DM}) vary from 0.58 Ga to 1.37 Ga. Compared with the host rocks, the MMEs are relatively homogeneous in isotopic composition, with I_{Sr} ranging from 0.705513 to 0.707275 and $\varepsilon_{Nd}(t)$ from −1.46 to 4.62. The MMEs have T_{DM} ranging from 0.49 Ga to 1.39 Ga. Geochemical and isotopic similarities between the MMEs and their host rocks demonstrate that the enclaves have mixed origins and were most probably formed by interactions between the lower crust- and mantle-derived magmas. Geochemical data, in combination with geodynamic evidence, suggest that a basic magma was derived from an enriched subcontinental lithospheric mantle (SCLM), presumably triggered by the influx of the hot asthenosphere. This magma then interacted with a crustal melt that originated from the dehydration melting of the mafic lower crust at deep crustal levels. Modeling based on Sr–Nd isotope data indicate that ~50% to 90% of the lower crust-derived melt and ~10% to 50% of the mantle-derived mafic magma were involved in the genesis of the early Oligocene magmas. In contrast, ~45%–65% of the mantle-derived mafic magma were incorporated into the lower crust-derived magma (~35%–55%) that generated the late Oligocene hybrid granitoid rocks. Early Oligocene granitoid rocks contain a higher proportion of crustal material compared to those that formed in the late Oligocene. It is reasonable to assume that lower crust and mantle interaction processes played a significant role in the genesis of these hybridgranitoid bodies, where melts undergoing fractional crystallization along with minor amounts of crustal assimilation could ascend to shallower crustal levels and generate a variety of rock types ranging from diorite to granite.

* Corresponding author.
E-mail address: rashid@modares.ac.ir (N. Rashidnejad-Omran).
Peer-review under responsibility of China University of Geosciences (Beijing).

https://doi.org/10.1016/j.gsf.2018.03.017

1. Introduction

The Zagros Orogenic Belt of Iran is part of the Alpine–Himalayan Belt that formed by continental collision after the closure of the Neo-Tethys Ocean between Arabia and Eurasia during the Cenozoic (Agard et al., 2005; Alavi, 2007; Mohajjel and Fergusson, 2014). It extends from the Turkish–Iranian border in the northwest to the Makran area in the southeast, where oceanic subduction is still active (Ellouz-Zimmermann et al., 2007; Smit et al., 2010). The Zagros Orogen consists of three parallel NW–SE trending tectonic zones, from southwest to northeast Iran (Mohajjel et al., 2003; Alavi, 2004; Agard et al., 2005), namely, the Zagros Fold-Thrust Belt (ZFTB), the Sanandaj–Sirjan Zone (SSZ) and the Central Iranian Magmatic Belt or Cenozoic Urumieh–Dokhtar Magmatic Belt (UDMB) (Fig. 1).

The UDMB is a 50–80 km wide Andean-type magmatic belt of Cenozoic intrusive and extrusive rocks resulting from oblique northeastward subduction of Neo-Tethyan ocean floor beneath Iran (Berberian and King, 1981; Berberian et al., 1982; Alavi, 1994; Shahabpour, 2007; Agard et al., 2011) followed by collision between the Arabian and Eurasian plates which began in the middle to late Miocene (Berberian and King, 1981; Şen et al., 2004; Chiu et al., 2013). The final closure of the Neo-Tethys, and the collision between Arabia and Central Iran took place during the Neogene (Berberian and Berberian, 1981; Berberian et al., 1982; Agard et al., 2011; Ballato et al., 2011; Verdel et al., 2011). Subduction-related igneous activity in Iran has been continuous from the Cretaceous to Recent, but maximum magmatic activity occurred between the Eocene and Oligocene (Berberian and King, 1981; Amidi et al., 1984).

To understand the magmatic history of granitoids within the UDMB and their significance in the geodynamic evolution of the area, in this paper, we report petrographical, and whole-rock elemental and isotopic geochemical features, and U-Pb zircon ages

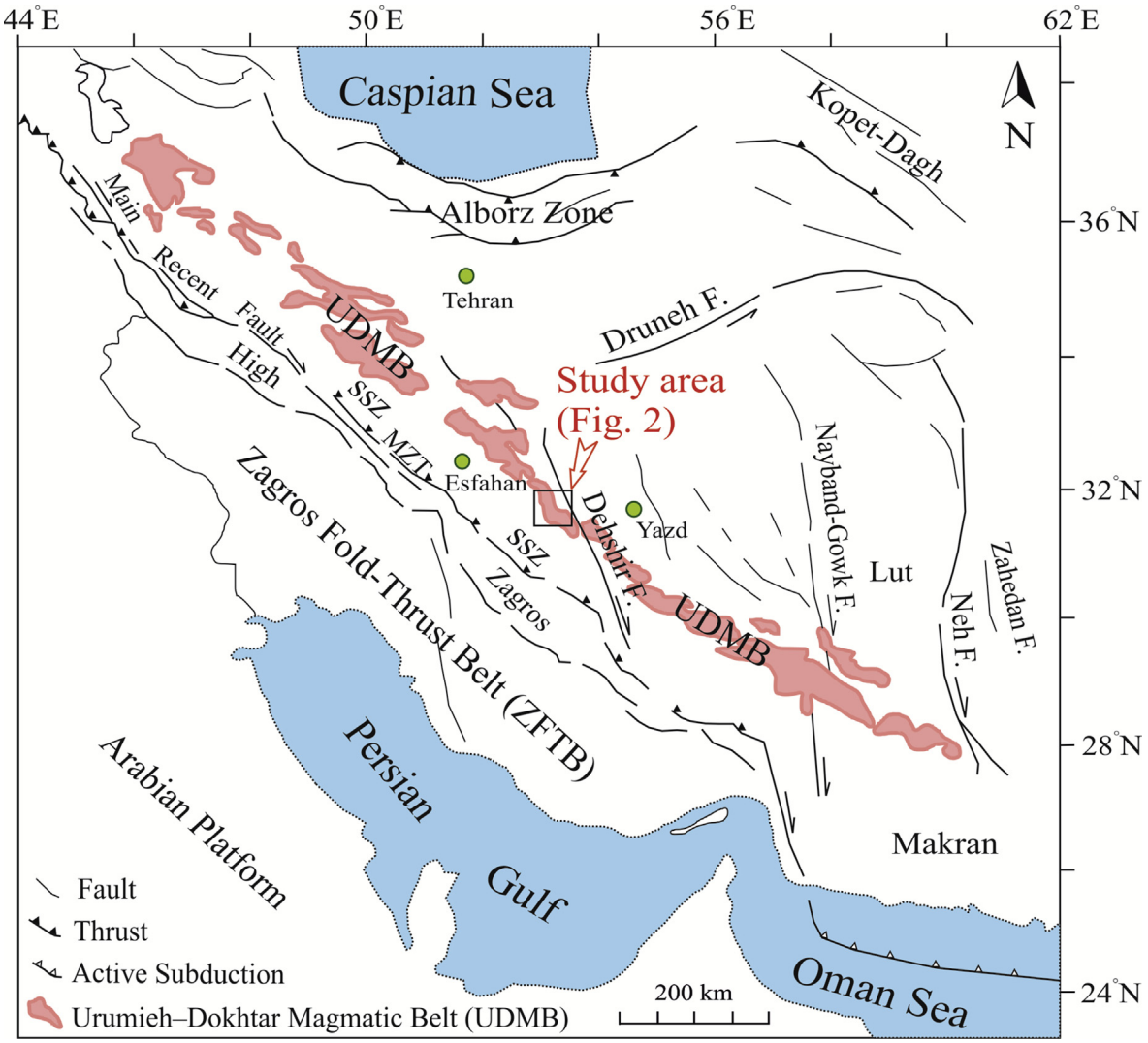

Figure 1. Tectonic zones of the Zagros Orogenic Belt. UDMB: Urumieh–Dokhtar Magmatic Belt, SSZ: Sanandaj–Sirjan Zone, MZT: Main Zagros Thrust, ZFTB: Zagros Fold-Thrust Belt. Small square marks the location of study area shown in Fig. 2.

of MMEs and their host granitoids from the NPC located within the central part of the UDMB. Field and petrographical evidence from the NPC strongly infer magma mingling/mixing processes and suggest the existence of more than one magmatic source in the genesis of these rocks. End member source compositions, however, are unknown for many plutons, including the NPC. A detailed study on such igneous complexes, therefore, could improve our understanding of their genesis, including the relative contribution of mantle- and crust-derived melts. In this study, the contribution of end-member compositions and key magmatic processes involved in the genesis of the NPC are discussed, which includes a detailed discussion on mingling/mixing, assimilation and fractional crystallization processes in the NPC using whole-rock elemental and Sr-Nd isotope data from the host granitoids and MMEs. Geochemical features as well as zircon U-Pb ages are also described for both, host rocks and MMEs. Lastly, the data are evaluated in terms of the NPC's significance in terms of the geodynamic evolution of the area, specifically its origin and evolution in subduction or collision-related settings during the Zagros orogeny.

2. Geological setting

The Nodoushan Plutonic Complex (NPC) outcropping between 31°42′–32°00′N and 53°15′–53°30′E is a part of the Cenozoic Plutonic Belt within the central UDMB, in an area bounded by the Nain-Dehshir Fault (NDF) and Borna Fault (Fig. 2).

The oldest stratigraphic units in the study area are dolomites and dolomitic limestones belonging to the Permian Jamal Formation, which are overlain by the early Jurassic Shemshak Formation, composed of shales and sandstones. These units are overlain by the early Cretaceous Sangestan Formation comprising shales, sandstones, conglomerates and orbitolina limestone, and then by Eocene andesitic to rhyodacitic calc-alkaline volcanic and subvolcanic rocks, with pyroclastics on the top. These units were intruded by the NPC investigated in this paper (Fig. 2).

The two groups of NPC rocks described here are felsic (granite and granodiorite) and intermediate (diorite and diorite porphyry), based on field and petrographic observations, especially modal mineral proportions. The diorites (Di in Fig. 2) are exposed as distinct bodies in the western part of the study area and occur as small separated ridges with low height. They intruded into the alternation of sandstone and conglomerate of the lower Cretaceous Sangestan Formation which is the oldest rock of the NPC based on field observations. Accordingly, the age of the diorite was described as post-Cretaceous (Ghalamghash and Mohammadiha, 2005). The granodiorite and diorite porphyry intrusives (Gd and Dip, in Fig. 2) cut through Eocene volcanic, sub-volcanic and pyroclastic rocks in the northern, central and southern parts of the study area. The granite, widely exposed as interconnected hilly lands with smooth erosional features, intruded into the Eocene volcanic, sub-volcanic and pyroclastic rocks (Gr in Fig. 2). Field relationships indicate a post-Eocene age for granite, granodiorite and diorite porphyry

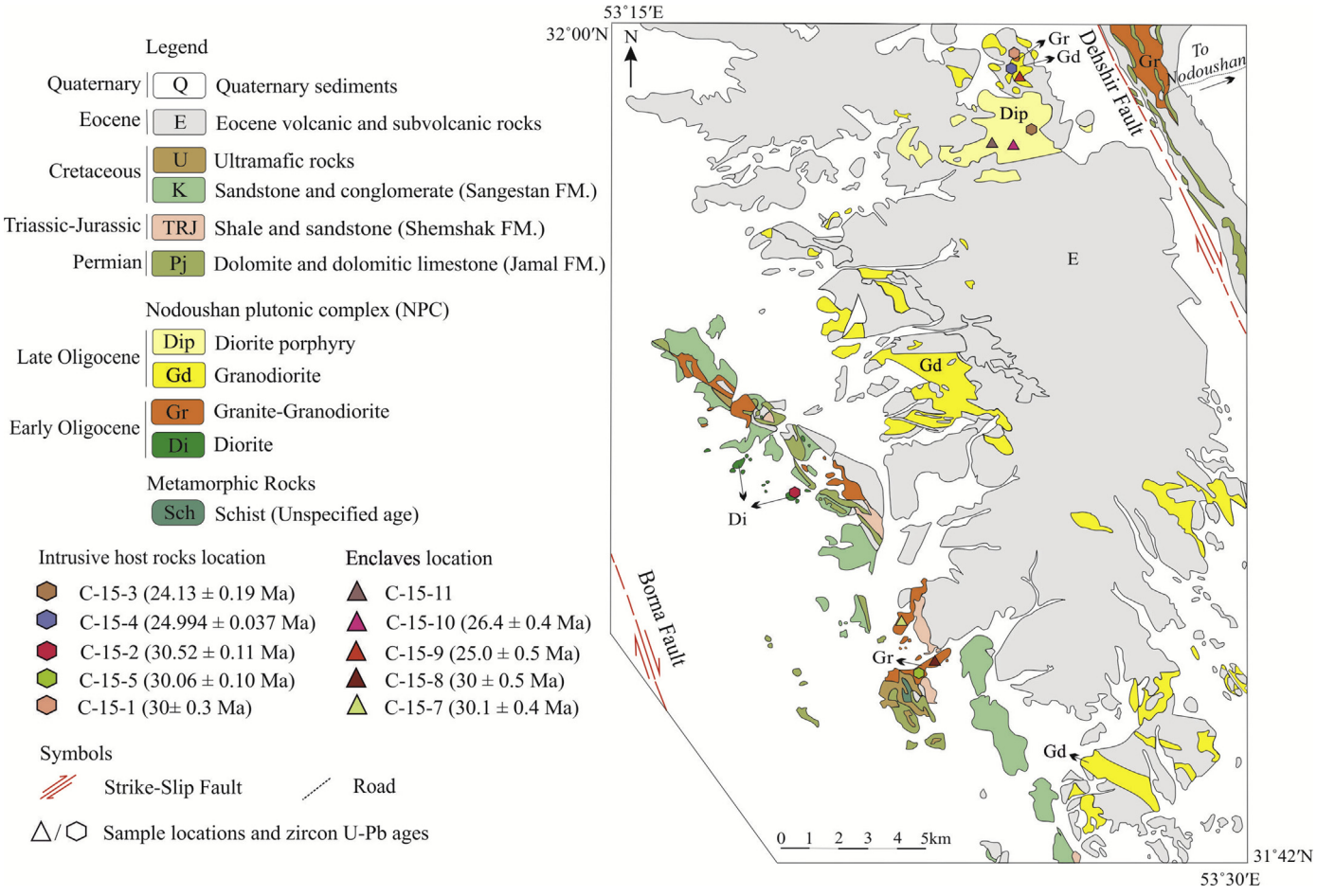

Figure 2. Simplified geological map of the Nodoushan Plutonic Complex (modified after Ghalamghash and Mohammadiha, 2005) with sample locations and U–Pb ages from this study. Host rocks include diorite porphyry (C-15-3), granodiorite (C-15-4), diorite (C-15-2) and granite (C-15-5 and C-15-1); enclaves include diorite (C-15-7), monzodiorite (C-15-8), diorite (C-15-9), gabbroic diorite (C-15-10) and diorite (C-15-11).

(Ghalamghash and Mohammadiha, 2005). Diorite porphyry and granodiorite form about ~70% of the mass volume of the NPC. Granite never exceeds 25% by volume, and diorite occupies less than 10% of the volume. Contact relations among the rocks are transitional. In addition, in the northern part, a small granitic body is surrounded by granodiorite. These granites are strongly silicified and alteration products like hematite and limonite are visible within them (Gr in Fig. 2). The Eocene volcanic rocks are metamorphosed and/or hydrothermally altered along their contacts with the intrusive bodies (e.g. epidotization and chloritization).

Widespread but heterogeneous distribution of MMEs within the intrusives are well-defined in the field. The MMEs are mainly concentrated in the diorite porphyry and granodiorite intrusives, and also in some parts of the granitic intrusions (Fig. 4A, B, and C). On the other hand, the post-Cretaceous dioritic intrusions are enclave-free. The MMEs are fine-grained compared to the host rocks. Compositionally, the light to dark grey colored MMEs are mainly diorite, monzodiorite and infrequently, gabbroic diorite. The MMEs are commonly 3 mm to 50 cm in size, and rarely up to 1 m across. Absence of a chilled margin at contacts between the MMEs and the hosts reflect that there is no major thermal contrast between them. The contacts with their hosts are usually sharp, crenulated, rounded or irregular, and occasionally diffuse (with no signs of deformation).

3. Analytical methods

3.1. Geochronological analyses

In this study, two different U-Pb dating methods on zircon separates were performed. They are Isotope Dilution Thermal Ionization Mass Spectrometry (ID-TIMS) and Laser-Ablation Inductively Coupled Plasma Mass Spectrometry (LA-ICP-MS). The results from both methods are evaluated in combination. In the first technique, the U-Pb analyses were accomplished by ID-TIMS at the University of Oslo, Norway (Table 1). Rock samples were crushed in a jaw crusher, pulverized in a blade mill, and then passed on a Wilfley table for a first enrichment step of the heavy minerals. Zircon grains were then concentrated by a combination of magnetic separation and heavy liquids. After hand-picking under a binocular microscope, the zircon grains were subjected to chemical abrasion (Mattinson, 2005). Dissolution was done in Krogh-type dissolution vessels at 195 °C in HF, together with a mixed $^{202}Pb/^{205}Pb/^{235}U$ tracer. The solution was passed through an anion exchange resin to purify Pb and U before performing ID-TIMS (Krogh, 1973) using a Finnigan-MAT 262 spectrometer at the Department of Geosciences, University of Oslo, Norway (Corfu, 2004). Blank corrections were ≤2 pg for Pb and 0.1 pg for U. The initial Pb correction was done using compositions calculated with the Stacey and Kramers (1975) model. The decay constants applied are those of Jaffey et al. (1971). Plots and regression analyses were done using the Isoplot program (Ludwig, 1999). All uncertainties relative to the analyses and ages are given at the 2σ level.

In the second technique, six samples (including enclaves and one sample of a granitic host rock in the northern part of the region that was surrounded by granodiorite) from the NPC were selected for U–Pb zircon dating. Zircons were extracted from whole–rock samples using standard techniques of density and magnetic separation, and then by handpicking under a binocular microscope, at the Langfang Regional Geological Survey, Hebei Province, China. These handpicked zircons were examined under transmitted and reflected light with an optical microscope. To reveal their internal structures, cathodoluminescence (CL) images were obtained using a JEOL scanning electron microscope housed at the Institute of Geology and Geophysics, Chinese Academy of Sciences in Beijing, China. Distinct domains within the zircons were selected for analysis, based on the CL images. LA-ICP-MS-based zircon U–Pb analyses were performed using an Agilent

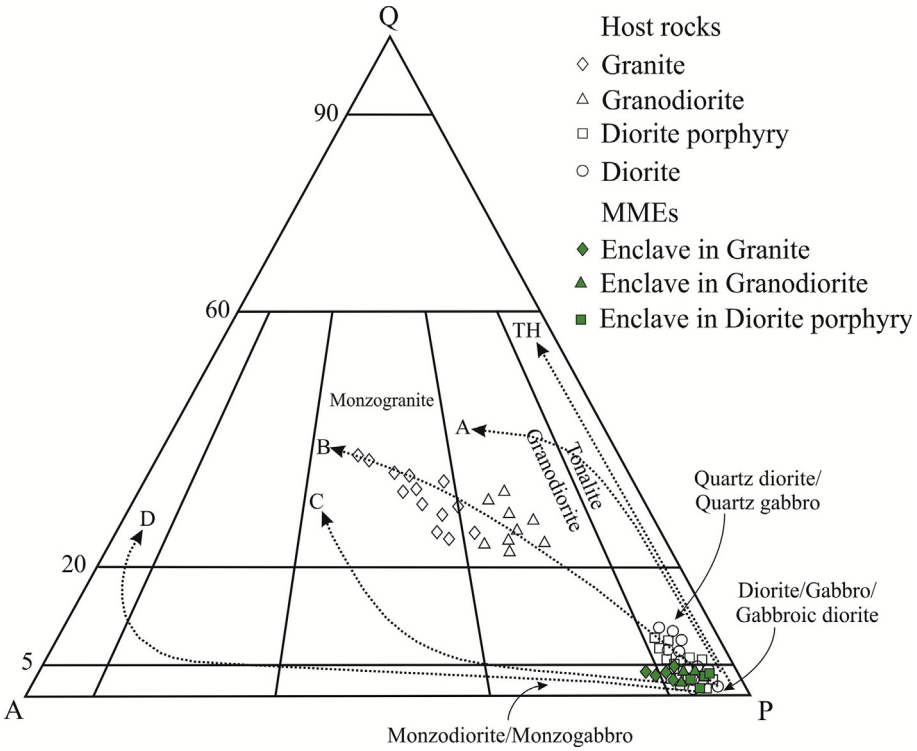

Figure 3. QAP diagram (Streckeisen, 1976) with geochemical trends (dashed arrows) of Lameyre and Bowden (1982) for the Nodoushan Plutonic Complex. A = calc-alkaline-trondhjemite (low K), B = calc-alkaline-granodiorite (medium K), C = calc-alkaline-monzonite (high K), D = alkaline and peralkaline, and TH = tholeiite.

7500a ICP-MS equipped with a 193 nm laser, housed at the State Key Laboratory of Geological Processes and Mineral Resources, China University of Geosciences, Wuhan, China. Zircon 91500 was used as an external standard for age calibration, and NIST SRM 610 silicate glass was applied for instrument optimization. The crater diameter was 32 μm during the analyses. For details on instrument settings and analytical procedures, see Yuan et al. (2004). The ICP-MS-DataCal (Ver. 6.7; Liu et al., 2008, 2010) and Isoplot (Ver. 3.0; Ludwig, 2003) programs were used for data reduction. Correction for common Pb was made following Andersen (2002). Errors on individual analyses by LA-ICP-MS are quoted at the 1σ level, while errors on pooled ages are quoted at the 95% (2σ) confidence level. The dating results are presented in Supplementary Table 1.

3.2. Geochemical analyses

A total of 200 rock samples were collected from the NPC. The modal mineralogy of 60 samples was determined by point counting with a Swift automatic counter fitted to a polarizing microscope. On each thin section a total of 1250–1500 points were counted, and modes were normalized to 100% (Table 2). After petrographical investigation, twentyseven whole-rock samples were analyzed for major and minor oxides, and trace elements including rare earth elements (REEs). After a petrographic inspection to ensure freshness, rock samples were crushed in specially designed steel jaw crushers and then powdered in a tungsten carbide ball mill to a grain size of <200 mesh. These analyses were performed by Inductively Coupled Plasma Optical Emission Spectrometry and Inductively Coupled Plasma Mass Spectrometry ICP-OES and ICP-MS, respectively) at the Central Laboratory (MERLAB), Middle East Technical University (METU, Ankara; Supplementary Table 2). The samples were digested using a three-step procedure in a high-pressure model of Anton Paar Multiwave 3000 rotor XF100-8. During the first step of the procedure, 0.3 g of powdered sample was left to ramp for 5 min after adding 1 mL HNO_3, 1 mL HCl and 3 mL HF, and held for 5 min in a multiwave. In the second step, complexation was achieved by adding 18 mL of 5% boric acid to the mixture, leaving it to ramp for 5 min, followed by holding for 15 min in the multiwave. In the third step, the solution was made up to 50 mL using de-ionized water. The analyses were performed with a detection limit of 0.01–10 ppm. Precision and accuracy for the data were calculated using the standard deviation of the mean (±SD) and relative standard deviation (%RSD) of replicate unknown samples and known reference materials. Precision of duplicate analyses were better than 1.2% RSD for SiO_2 and better than 0.28% RSD for the rest of the oxides and trace elements. C, H, N, S were measured by a LECO element analysis instrument to determine loss on ignition (LOI) at MERLAB, METU.

3.3. Sr and Nd isotopic analyses

Isotopic analyses for strontium and neodymium of fifteen samples were performed by a Thermo-Fisher Triton Multi-Collector Thermal Ionization Mass Spectrometer with static multi-collection at the Radiogenic Isotope Laboratory, MERLAB, METU (Ankara; Table 3). Chemical treatment, chromatography and sample loading were performed in a class-100 clean laboratory by using ultrapure chemical agents. The analytical procedures described by Köksal and Göncüoğlu (2008), and Köksal et al. (2017) were followed to concentrate the isotopes. Powdered samples (ca. 80 mg) were weighed and transferred into Savillex PFA vials. Samples were leached with 4 mL of 52% HF for 4 day at >100 °C on a hot plate. Digested samples were dried and then dissolved overnight in 4 mL 6 N HCl at >100 °C on a hot plate. Strontium was separated in Teflon columns with 2.5 N HCl as the medium, and 2 mL BioRad AG50 W-X8 (100–200 mesh) resin. The REE fraction was diluted using 6 N HCl after elution of Ba with 2.5 N HNO_3. Strontium was loaded on single Re-filaments with Ta-activator and 0.005 N H_3PO_4. $^{87}Sr/^{86}Sr$ data was normalized to $^{86}Sr/^{88}Sr = 0.1194$. The Sr standard NIST SRM 987 was measured as 0.710232 ± 0.000005 ($n = 2$). Strontium isotopic compositions were corrected for instrumental bias. Neodymium was separated from the REE fraction in Teflon columns with 0.22 N HCl as the medium, using 2 mL biobeads (Bio Rad) coated with HDEHP (bis-ethyexyl phosphate). Neodymium was loaded on double Re-filaments with 0.005 N H_3PO_4. $^{143}Nd/^{144}Nd$ data are normalized to $^{146}Nd/^{144}Nd = 0.7219$. The standard Nd La Jolla was measured as 0.511851 ± 0.000005 ($n = 2$). No corrections were applied to Nd isotopic compositions for instrumental bias. Analytical uncertainties are given at 2σ level. During the analyses BCR-1 USGS and AGV-1 standards were processed at the same conditions that gave $^{87}Sr/^{86}Sr = 0.705030 \pm 0.000004$ and $^{143}Nd/^{144}Nd = 0.512627 \pm 0.000003$ ratios, and $^{87}Sr/^{86}Sr = 0.703992 \pm 0.000004$ and $^{143}Nd/^{144}Nd = 0.512785 \pm 0.000003$ ratios, respectively.

4. Results

4.1. Petrographic features

4.1.1. Granitoid host rocks

The petrographic characteristics of the Nodoushan granitoids are presented in Table 2. The rocks of the NPC plot in the fields of granite, granodiorite and diorite-quartz diorite with a medium-K calc-alkaline differentiation trend (Lameyre and Bowden, 1982) in the QAP (quartz-alkali feldspar-plagioclase) modal classification diagram (Streckeisen, 1976) (Fig. 3). All the rock units share several common petrographic features and are described together. The main rocks of the NPC are holocrystalline and predominantly medium-grained (Fig. 4A, B and C), containing prismatic amphibole or larger acicular amphibole (Fig. 4D) and plagioclase grains that display oscillatory zoning (Fig. 4E) in a finer-grained matrix of plagioclase (25%–70%), K-feldspar (3%–40%), quartz (2%–38%), amphibole (1%–22%), biotite (0–12%), pyroxene (cpx; 0–8%) and iron–titanium oxides (1%–7%), in descending order of abundance. Important mafic constituents are represented by amphibole, biotite and pyroxene, with amphibole predominant over biotite and pyroxene. Most of the coarse plagioclase crystals display oscillatory zoning and prismatic-cellular growth (Fig. 4E), which can be attributed to magma mixing (e.g. Vernon, 1990; Hibbard, 1991; Waight et al., 2000; Aslan, 2005), with corroded boundaries resulting from resorption-regrowth processes. Oscillatory zoning in plagioclase indicates variation in the crystallization conditions (Holten et al., 2000). In addition, some plagioclase phenocrysts poikilitically envelope fine plagioclase, hornblende and/or magnetite crystals together with apatite inclusions (Fig. 4E and F); a feature that has been considered evidence for magma mixing (Akal and Helvaci, 1999; Aslan, 2005). Lath-shaped plagioclase crystals are commonly observed. Quartz and K-feldspar (orthoclase and microcline) are present in variable proportions. Both minerals, typically anhedral, occur as interstitial phases.

Coarse crystals of clinopyroxene and hornblende are the most common mafic minerals in diorite porphyries of the NPC. Pyroxene varieties of augitic diopside are commonly present as euhedral phenocrysts (Fig. 4G). In some cases, euhedral phenocrysts of augitic clinopyroxene and hornblende poikilitically enclose fine-grained plagioclase and accessory phases. Optical zoning is clear in clinopyroxene phenocrysts (Fig. 4G). Biotite occurs as euhedral/subhedral platy crystals with variable sizes. Coarse plates contain inclusions of zircon and opaque minerals (Fig. 4H). It is strongly pleochroic, from pale straw yellow to reddish brown. Granophyric

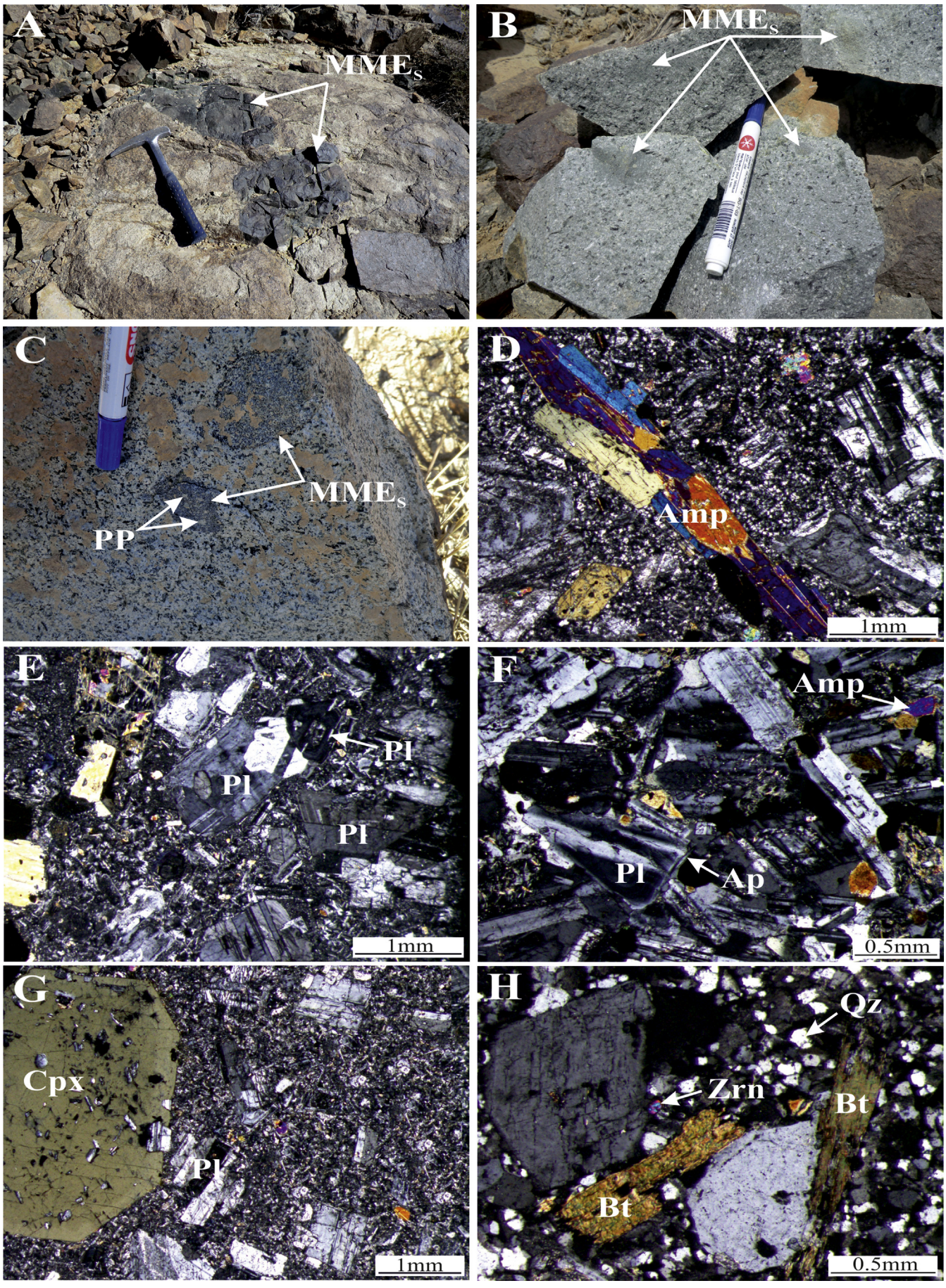
A
MMEs
B
MMEs
C
MMEs
PP
D
Amp
1mm
E
Pl
Pl
Pl
1mm
F
Amp
Pl
Ap
0.5mm
G
Cpx
Pl
1mm
H
Qz
Zrn
Bt
Bt
0.5mm

Table 1
ID-TIMS U-Pb data for zircons from the Nodoushan plutonic complex.

Fraction[a]	Weight (ug)	U (ppm)	Th/U[b]	Pb_c[c] (pg)	$^{206}Pb/^{204}Pb$[d]	$^{207}Pb/^{235}U$[e]	±2σ [abs]	$^{206}Pb/^{238}U$[e]
Sample C-15-3 (N34) Diorite porphyry (31°57′50.8″N, 53°24′35.9″E)								
Zrn eu lp 7gr	18	80	0.70	5.9	78	0.02550	0.00154	0.003864
Zrn eu sp 1gr	53	47	0.51	3.3	198	0.02423	0.00070	0.003752
Zrn eu tips 2gr	15	54	0.52	1.5	142	0.02380	0.00154	0.003763
Zrn eu eq 2gr	26	62	0.47	3.3	132	0.02377	0.00106	0.003738
Sample C-15-5 (N52) Granite (31°46′32.7″N, 53°22′51.9″E)								
Zrn eu sp 8gr	53	244	0.70	2.4	1583	0.03007	0.00016	0.004682
Zrn eu tip 10gr	31	351	0.78	5.5	592	0.03012	0.00023	0.004667
Sample C-15-2 (N8) Diorite (31°49′49.0″N, 53°19′14.1″E)								
Zrn eu sp 7gr	21	317	0.89	3.9	524	0.03057	0.00031	0.004752
Zrn eu flat/lp 14gr	36	309	0.94	2.4	1371	0.03062	0.00018	0.004746
Zrn eu lp-fr 11gr	32	294	0.97	3.6	790	0.03056	0.00023	0.004738
Sample C-15-4 (N164) Granodiorite (31°59′4.7″N, 53°24′27.7″E)								
Zrn eu lp-sp 12gr	39	122	0.61	2.5	482	0.02481	0.00037	0.003887
Zrn eu sp 6gr	54	119	0.72	5.4	310	0.02497	0.00037	0.003884
Zrn eu eq 12gr	37	113	0.73	0.9	1148	0.02494	0.00023	0.003882

Fraction[a]	±2σ [abs]	rho	$^{207}Pb/^{206}Pb$[e]	±2σ [abs]	$^{206}Pb/^{238}U$[e] (Ma)	±2σ	$^{207}Pb/^{235}U$[e] (Ma)	±2σ
Sample C-15-3 (N34) Diorite porphyry (31°57′50.8″N, 53°24′35.9″E)								
Zrn eu lp 7gr	0.00002	0.39	0.047865	0.00280	24.86	0.14	25.57	1.52
Zrn eu sp 1gr	0.00001	0.54	0.046841	0.00128	24.14	0.07	24.31	0.69
Zrn eu tips 2gr	0.00001	0.74	0.045865	0.00284	24.21	0.10	23.88	1.52
Zrn eu eq 2gr	0.00001	0.61	0.046130	0.00197	24.05	0.09	23.86	1.05
Sample C-15-5 (N52) Granite (31°46′32.7″N, 53°22′51.9″E)								
Zrn eu sp 8gr	0.00001	0.62	0.046575	0.00021	30.11	0.07	30.08	0.16
Zrn eu tip 10gr	0.00001	0.52	0.046815	0.00031	30.01	0.07	30.13	0.22
Sample C-15-2 (N8) Diorite (31°49′49.0″N, 53°19′14.1″E)								
Zrn eu sp 7gr	0.00001	0.48	0.046668	0.00043	30.56	0.08	30.58	0.31
Zrn eu flat/lp 14gr	0.00001	0.60	0.046801	0.00023	30.52	0.08	30.63	0.18
Zrn eu lp-fr 11gr	0.00001	0.53	0.046785	0.00031	30.47	0.08	30.57	0.23
Sample C-15-4 (N164) Granodiorite (31°59′ 4.7″N, 53°24′ 27.7″E)								
Zrn eu lp-sp 12gr	0.00001	0.48	0.046293	0.00064	25.01	0.06	24.89	0.37
Zrn eu sp 6gr	0.00001	0.44	0.046627	0.00064	24.99	0.07	25.04	0.36
Zrn eu eq 12gr	0.00001	0.49	0.046603	0.00038	24.98	0.07	25.02	0.22

[a] All zircon grains chemically abraded before analysis; eu = euhedral; lp = long prismatic; sp = short prismatic; eq = equant; fr = broken grain; Xgr = number of grains in fraction.
[b] Th/U model ratio inferred from 208/206 ratio and age of sample.
[c] Total amount of common Pb (initial + blank).
[d] Raw data corrected for fractionation.
[e] Corrected for fractionation, spike, blank and disequilibrium due to ^{230}Th-excess (Scharer, 1984), assuming a Th/U of the magma of 4; error calculated by propagating the main sources of uncertainty: ages are also normalized to the NIGL value of ET100 solution.

and myrmeritic textures are common in granitic rocks (Fig. 5A). Plagioclase tends to be an early, dominant phase. Some of them, moreover, are mantled by orthoclase forming anti-rapakivi texture (Fig. 5A). Apatite (as irregular blobs within other minerals such as plagioclase), titanite (primary and secondary), zircon (as prismatic crystals), and opaque minerals are accessory phases in all the rock types of the NPC. Effects of low-temperature rock alterations are noted. Plagioclase is influenced by sub-solidus alteration forming sericite, epidote and calcite. K-feldspar is locally altered to kaolinite. Biotites are locally replaced by chlorite, secondary titanite and magnetite along grain boundaries and cleavages. Some amphibole grains were altered to actinolite, chlorite and titanite, especially along the rims. Clinopyroxene is commonly replaced by hydrothermal veinlets filled with uralite.

Some features of I-type granitoids are revealed by the mineralogy of the NPC. For instance, hornblende is the common mafic mineral in all discussed intrusives whereas Al-rich phases such as garnet, cordierite, muscovite, etc. are absent. In addition, there is no monazite, and titanite is the prevailing accessory phase. The presence of apatite as inclusions is a common feature, considered to be typical in I-type granitoids, whereas apatite appears in the form of larger individual crystals in S-type granitoids. Modal distributions of S-type granitoids are similar to those of I-type, but S-type fall in the adamellite/granite range and I-type into the monzodiorite/tonalite/granodiorite range (Hine et al., 1978).

4.1.2. Magmatic microgranular enclaves (MMEs)

Minerals in the enclaves are generally the same as those of the host granitoids but they have different abundances. In comparison with the host rocks, the MMEs are fine-grained and their compositions vary from diorite to monzodiorite with minor gabbroic diorite (in the QAP diagram, Fig. 3). The MMEs contain higher ferromagnesian phases, plagioclase, lower quartz and K-feldspar than those of the host rocks (Table 2). They are composed of plagioclase (56%–76%), amphibole (6%–20%), biotite (1%–8%), pyroxene (0–6%), orthoclase (3%–7%), quartz (2%–5%) and Fe-Ti oxides (2%–4%). Phenocrysts in the MMEs are plagioclase, hornblende, clinopyroxene, biotite and minor quartz (Fig. 5B–F), in a fine-grained matrix typically showing microlitic porphyric and microgranular textures (Fig. 5B–D). Some large subhedral quartz grains are surrounded by early-crystallized phases including fine-grained hornblende (quartz ocelli; Fig. 5B and D). Plagioclases in the MMEs occur as anhedral to subhedral, rounded/corroded and

Figure 4. (A–C) Macroscopic view of magmatic microgranular enclaves (MMEs) within the host rocks (granite, diorite porphyry and granodiorite, respectively) and (D–H) photomicrographs showing textural relationships of the host granitoid rocks. Mineral abbreviations are after Whitney and Evans (2010): amphibole (Amp), clinopyroxene (Cpx), plagioclase (Pl), biotite (Bt), quartz (Qz), apatite (Ap), zircon (Zrn) and plagioclase phenocryst (PP). All the microphotographs are shown in crossed polarized light (XPL).

Table 2
General petrographic features of the various rock-types from the Nodoushanplutonic complex.

Rock unit	Diorite (Diorite to Quartz-diorite) ($n = 12$)		Diorite porphyry (Diorite to Quartz-diorite porphyry) ($n = 14$)		Granodiorite ($n = 9$)		Granite (Granite–Granodiorite) ($n = 13$)		MMEs ($n = 12$)	
Textures	Hypidiomorphic-granular, locally poikilitic		Hypidiomorphic-porphyritic, weakly granular, locally poikilitic		Hypidiomorphic-granular to porphyritic, locally poikilitic		Granitic to porphyritic, locally Granophyric, myrmeritic, anti-rapakivic and poikilitic		Porphyritic with a fine-grained matrix, microlitic porphyritic and microgranular	
Grain size	Fine to medium		Medium to coarse		Medium to coarse		Fine to medium		Fine	
Modal min (%)	Min–max	Avg	Min–max	Avg	Min–max	Avg	Min–max	Avg	Min–max	Avg
Plagioclase	60–70	65	60–65	62.5	36–56	46	25–42	33.5	56–76	66
K-Feldspar	3–5	4	3–7	5	6–20	13	18–40	29	3–7	5
Quartz	3–10	6.5	2–10	6	21–33	27	25–38	31.5	2–5	3.5
Hornblende	15–22	18.5	1–20	10.5	1–11	6	1–3	2	6–20	13
Biotite	0–3	1.5	0–2	1	0–4	2	0–12	6	1–8	4.5
Pyroxene	0–2	1	0–8	4	0–5	2.5	–	–	0–6	3
Accessory phases	titanite, apatite, zircon and opaques		titanite, apatite, zircon and opaques		titanite, apatite, zircon and opaques		titanite, apatite, zircon and opaques		titanite, apatite, zircon and opaques	
Secondary minerals	sericite, epidote, chlorite, calcite and actinolite		sericite, epidote, chlorite, calcite, actinolite and uralite		sericite, epidote, chlorite, calcite, actinolite, uralite and clay minerals		sericite, epidote, chlorite, calcite, clay minerals, titanite and magnetite		sericite, epidote, chlorite, calcite and clay minerals	

Notes: n–sample number, Min–minimum values, Max–maximum values, Avg–average values and MMEs–Mafic Microgranular Enclaves.

zoned phenocrysts; and as laths in the groundmass of MMEs (Fig. 5B–D). Some plagioclase phenocrysts poikitically envelope hornblende and/or magnetite crystals together with apatite inclusions (Fig. 5C). In addition, phenocrysts of plagioclase and mafic phases cross the host-enclave boundary (Fig. 5E). Phenocrysts crossing (e.g. plagioclase) the host-enclave boundary in the samples suggest that they were mechanically transferred from the host granitoid magma to the enclave magma (Fig. 5E), during the mixing of basic and felsic magmas, while they behaved as liquids at depths. Low rheological contrasts between two magmas allow crystal transfer from a host magma into a basic magma (e.g. Barbarin and Didier, 1992; Waight et al., 2000; Perugini et al., 2003). In the other words, concentration of phenocrysts near the enclave/host contact (Fig. 5E and F) indicates that they are foreign to the enclaves. Such cases are usually interpreted as evidence of mineral exchange between host and mafic magma before enclave formation (Paterson et al., 2004).

The pyroxene variety of augitic diopside is commonly present as euhedral phenocrysts, with resorption and corrosion seldom seen as they occur very rarely in the enclaves with the granodioritic and diorite porphyry host rock (Fig. 5E). Amphibole is more abundant than biotite in the enclaves. The amphiboles are variably-sized crystals of single prismatic or acicular hornblende and actinolite. The smaller hornblende crystals occur as randomly-oriented individual matrix crystals, and more rarely as aggregates (Fig. 5B–F). Furthermore, biotite-bearing and biotite-free MMEs occur in the biotite-bearing and biotite-free host granitoids, respectively. The predominance of hydrous minerals (e.g. biotite and amphibole), reflect H_2O-rich melt compositions for both mafic enclaves and granitoid host rocks. In some cases, large plagioclases crosscut the enclave-host boundary (Fig. 5F). Worldwide, these features are considered to prove the liquid state of the enclaves upon their incorporation into a more felsic magma (e.g. Vernon, 1984; Perugini et al., 2003). Quartz and alkali feldspar are anhedral interstitial phases (Fig. 5G). Presence of poikilitic phenocrysts of K-feldspar in the enclaves suggest that they grow while they are surrounded by melt, allowing the mineral inclusions to periodically attach themselves to the faces of the growing crystals (Fig. 5G; Moore and

Table 3
Sm–Nd isotope compositions for the rocks from the Nodoushan plutonic complex.

Sample	AGE (Ma)	Rb (ppm)	Sr (ppm)	$^{87}Rb/^{86}Sr$	$^{87}Sr/^{86}Sr$	2σm	I_{Sr} (t)	Sm (ppm)	Nd (ppm)	$^{147}Sm/^{144}Nd$	$^{143}Nd/^{144}Nd$	2σm	ε_{Nd} (0)	$\varepsilon_{Nd}(t)$	$f_{Sm/Nd}$	T_{DM} (Ga)
Host rocks																
N7	30.52	25	451	0.1602	0.707616	18	0.707547	4.32	17.7	0.1477	0.512463	2	−3.41	−3.22	−0.25	1.33
N8	30.52	25	414	0.1745	0.707082	18	0.707006	4.12	17.6	0.1416	0.512767	3	2.52	2.73	−0.28	0.61
N159	24.994	22	355	0.1791	0.705268	12	0.705204	2.27	9.17	0.1498	0.512465	3	−3.37	−3.23	−0.24	1.37
N164	24.994	42	342	0.3549	0.706124	16	0.705998	1.91	8.42	0.1372	0.512764	2	2.46	2.65	−0.30	0.58
N34	24.13	25	349	0.2070	0.705519	5	0.705448	2.23	8.8	0.1533	0.512826	2	3.67	3.80	−0.22	0.58
N97	24.13	41	334	0.3548	0.705167	5	0.705045	2.04	8.92	0.1384	0.512746	2	2.11	2.29	−0.30	0.62
N69	30.06	113	241	1.3551	0.708538	20	0.707959	2.79	14.2	0.1189	0.512498	3	−2.73	−2.43	−0.40	0.88
N85	30.06	138	209	1.9082	0.706679	15	0.705864	2.16	13.1	0.0998	0.512539	2	−1.93	−1.56	−0.49	0.69
N52	30.06	114	260	1.2672	0.70676	5	0.706219	2.16	12.4	0.1054	0.512534	2	−2.03	−1.68	−0.46	0.73
MMEs																
Nd164 E^+	25	34	371	0.2649	0.706881	23	0.706787	2.52	9.77	0.1560	0.512739	1	1.97	2.10	−0.21	0.82
N107 E^+	25	39	454	0.2483	0.706282	22	0.706194	2.48	9.69	0.1548	0.512868	2	4.49	4.62	−0.21	0.49
N127 E^+	26.4	63	731	0.2491	0.705994	9	0.705901	4.97	23	0.1307	0.512615	2	−0.45	−0.23	−0.34	0.80
N129 E^+	26.4	79	565	0.4041	0.705665	8	0.705513	4.69	22	0.1290	0.512617	2	−0.41	−0.18	−0.34	0.78
N58 E^+	30.1	79	201	1.1359	0.707761	25	0.707275	4.86	18.3	0.1607	0.512556	3	−1.60	−1.46	−0.18	1.39
N48 E^+	30	57	267	0.6170	0.707308	11	0.707045	3.67	14.1	0.1575	0.512563	3	−1.46	−1.31	−0.20	1.30

Notes: $\varepsilon_{Nd} = (((^{143}Nd/^{144}Nd)_s/(^{143}Nd/^{144}Nd)_{CHUR} - 1) \times 10{,}000, f_{Sm/Nd} = (^{147}Sm/^{144}Sm)_s/(^{147}Sm/^{144}Sm)_{CHUR} - 1$, $(^{143}Nd/^{144}Nd)_{CHUR} = 0.512638$, and $(^{147}Sm/^{144}Sm)_{CHUR} = 0.1967$. The model ages were calculated using a linear isotopic ratio growth equation: $T_{DM} = 1/\lambda \times \ln(1 + ((^{143}Nd/^{144}Nd)_s - 0.51315)/((^{147}Sm/^{144}Nd)_s - 0.2137))$. Standard errors are for last 1 or 2σ (i.e., 0.000005 or 0.000025).

Sisson, 2008). They also exist as small inclusions in cellular plagioclase phenocrysts and as rims of prismatic plagioclase (Fig. 5D). It is interesting to note that apatites in MMEs are mainly acicular (or needle-like; Fig. 5H), with rare stubby inclusions, while the host granitoids only have euhedral stubby apatite. The enclaves show minor alteration of feldspar to kaolinite, sericite, epidote and calcite. Many amphiboles show alterations to actinolite, chlorite and iron-oxides. Occasionally, biotite shows alteration to chlorite. In some cases, secondary opaque minerals occur along cleavage planes.

Sharp, crenulated, rounded or irregular, and occasionally diffuse (with no signs of deformation) contacts between the MMEs and their host can be attributed to a mixing of mafic and felsic magmas (Perugini et al., 2004). Kim et al. (2002) stated that the hybrid melt zone is formed where felsic and mafic magmas interact through net-veining by episodic mixing of both mafic and felsic melts. The degree of thermal, rheological and compositional contrast of co-existing mafic and felsic magmas will govern their interactions and the development of the hybrid magma zone at depth (Kumar et al., 2004).

4.2. Zircon geochronology

Four samples of the host rock from the NPC were selected for U-Pb zircon ID-TIMS dating (Table 1). They include diorite porphyry (C-15-3), diorite (C-15-2), granodiorite (C-15-4) and granite (C-15-5). The locations of the analyzed samples are marked in Fig. 2. New U–Pb zircon ages reveal that the NPC was assembled incrementally over ca. 5 m.y., during two main episodes at 30.52 ± 0.11 Ma and 30.06 ± 0.10 Ma in the early Oligocene (middle Rupelian) for dioritic and granite intrusives, and at 24.994 ± 0.037 Ma and 24.13 ± 0.19 Ma in the late Oligocene (latest Chattian) for granodioritic and diorite porphyry units, respectively (Shahsavari Alavijeh et al., 2017). In the next step, six samples (including enclaves and one sample of a granitic host rock) from the NPC were selected for LA-ICP-MS zircon U-Pb dating (Supplementary Table 1 and Fig. 7). Zircon grains exhibit pyramidal terminations and oscillatory zoning, indicating a magmatic origin. Zircons are variable both in terms of morphology and internal textures. These features reflect the geologic history of the mineral, especially the relevant episode(s) of magmatic crystallization. Cathodoluminescence (CL) images of the NPC samples show a more uniform core and wide bright rims with oscillatory zoning (Fig. 6). Zircons grains are mostly euhedral, short-prismatic with lengths up to 150 μm and aspect ratios ranging from approximately 1.7 to 2.5, although some zircons show a length-to-width ratio of up to 1:3. Zircons from the monzodiorite and diorite enclaves yielded concordant ages of 30 ± 0.5 Ma and 30.1 ± 0.4 Ma, respectively (Fig. 7A and B). These enclaves occurred in the granitic intrusions (30.06 ± 0.10 Ma). On the other hand, the dioritic intrusions (30.52 ± 0.11 Ma) are enclave-free. Ages of 25.0 ± 0.5 Ma and 26.4 ± 0.4 Ma were obtained for the diorite and gabbroic dioriteen claves (Fig. 7C and D). These enclaves are mainly concentrated in the granodiorite and diorite porphyry intrusives (late Oligocene), respectively. Meanwhile, an age of 30 ± 0.3 Ma was obtained for the granitic host rock in the northern part of the region that was surrounded by granodiorite (Fig. 7F). These results are in agreement with stratigraphic and field observations, indicating that the Nodoushan intrusions intruded into early Cretaceous units of the Sangestan Formation and Eocene calc-alkaline volcanic and sub-volcanic rocks. However, in the dioritic enclaves (Fig. 7E), the data indicate the presence of an inherited component. In this regard, the analysis of inherited zircons from the NPC are used to investigate the origin and continental affinity of the basement in the central part of the UDMB (Supplementary Table 1 and Fig. 7D and E). The inherited grains yield mainly Neoproterozoic to Cambrian ages between 873 Ma and 508 Ma, probably reflecting a provenance from, or assimilation of Neoproterozoic rocks during the generation and ascension of the magmas.

The basement underlying the central part of UDMB is composed of a continental fragment with Gondwanan affiliation, as seen in the Alborz Mountains, Central Iran, the Sanandaj-Sirjan zone (Hassanzadeh et al., 2008), and also the Kashan Plutonic Complex in Central Iran (Honarmand et al., 2013). Prior studies on lower crustal xenoliths of Arabia demonstrate that they form a part of a gabbroic intrusive complex that underlies the Arabian Plate and may show mafic roots of one or more arc complexes of Pan-African (Neoproterozoic) age (Al-Mishwat and Nasir, 2004). Recent geochronological dating for the granites and orthogneisses from basement units show an age range from the Ediacaran (late Neoproterozoic) to early Cambrian (Ramezani and Tucker, 2003; Hassanzadeh et al., 2008), matching the mostly juvenile Arabian–Nubian shield and Peri-Gondwanan terranes that formed after the main phase of the Pan-African orogenesis. Indeed, this late Neoproterozoic-early Cambrian basement in Iran was associated with an extensive magmatic arc that extends along the Proto-Tethyan margin of the Gondwana supercontinent. The UDMB basement may be an isolated remnant of that margin which is currently embedded within the Alpine-Himalayan orogenic belt. The results from inherited zircons show that the basement underlying the study area is composed of continental fragments with Gondwanan affiliation. Accordingly, inherited zircons (~500–800 Ma) in the Oligocene granitoids indicate involvement of older crust (with Arabian affinity), in the generation of younger plutonism in the Nodoushan magmatic segment.

4.3. Major and trace element geochemistry

Representative chemical analyses are listed in Supplementary Table 2. In the classification diagram of De la Roche et al. (1980), the host rocks of the NPC plot mainly in the fields of granodiorite, tonalite and diorite; their MMEs plot in the fields of diorite to monzodiorite, and more rarely as gabbroic diorite (Fig. 8). The host rocks are metaluminous with ASI [= molar Al_2O_3/($CaO + K_2O + Na_2O$)] ranging from 0.81 to 1.01 and are of I-type character; the MMEs are metaluminous (with ASI = 0.79–0.91; Supplementary Table 2 and Fig. 9A). All samples are of sub-alkaline affinity and belong to the medium-to-high-K calc-alkaline series (Fig. 9B). Accordingly, the R_1–R_2 classification diagram of the pluton, developed by Batchelor and Bowden (1985) to explain specific tectonic settings, suggests a pre-plate collision phase for the Oligocene NPC (Fig. 9C). In the Yb + Ta vs. Rb diagram (Pearce et al., 1984), all of the NPC samples appear in the volcanic arc granite (VAG) field due to their low values of Ta, Yb, Nb and Y (Fig. 9D).

As previously mentioned, different parts of the NPC, like other igneous rocks found in the UDMB, have geochemical signatures indicating that they formed in a volcanic arc setting in the northern margin of the Neo-Tethys, as part of an active continental margin (Fig. 9E). Major and trace element variations are shown in Harker plots (Fig. 10). Though the MMEs and their host rocks display a wide range in SiO_2 content, the MMEs (with SiO_2 = 47.73–57.36 wt.%, Mg# = 42.15–53.04; Supplementary Table 2) are less differentiated than the host rocks (with SiO_2 = 56.51–72.35 wt.%; Mg# = 26.29–50.86). Linear trends are apparent for major element oxides of the enclaves and host granitoids (Fig. 10); here again, enclaves are more basic than the host rocks. All the rocks define a similar variation trend without a compositional gap in most of the Harker plots (Fig. 10). Al_2O_3, MgO, Fe_2O_3, CaO, TiO_2, P_2O_5 and MnO contents linearly decrease with increasing SiO_2, while K_2O and Na_2O increase. Strong correlations between some major oxides and SiO_2

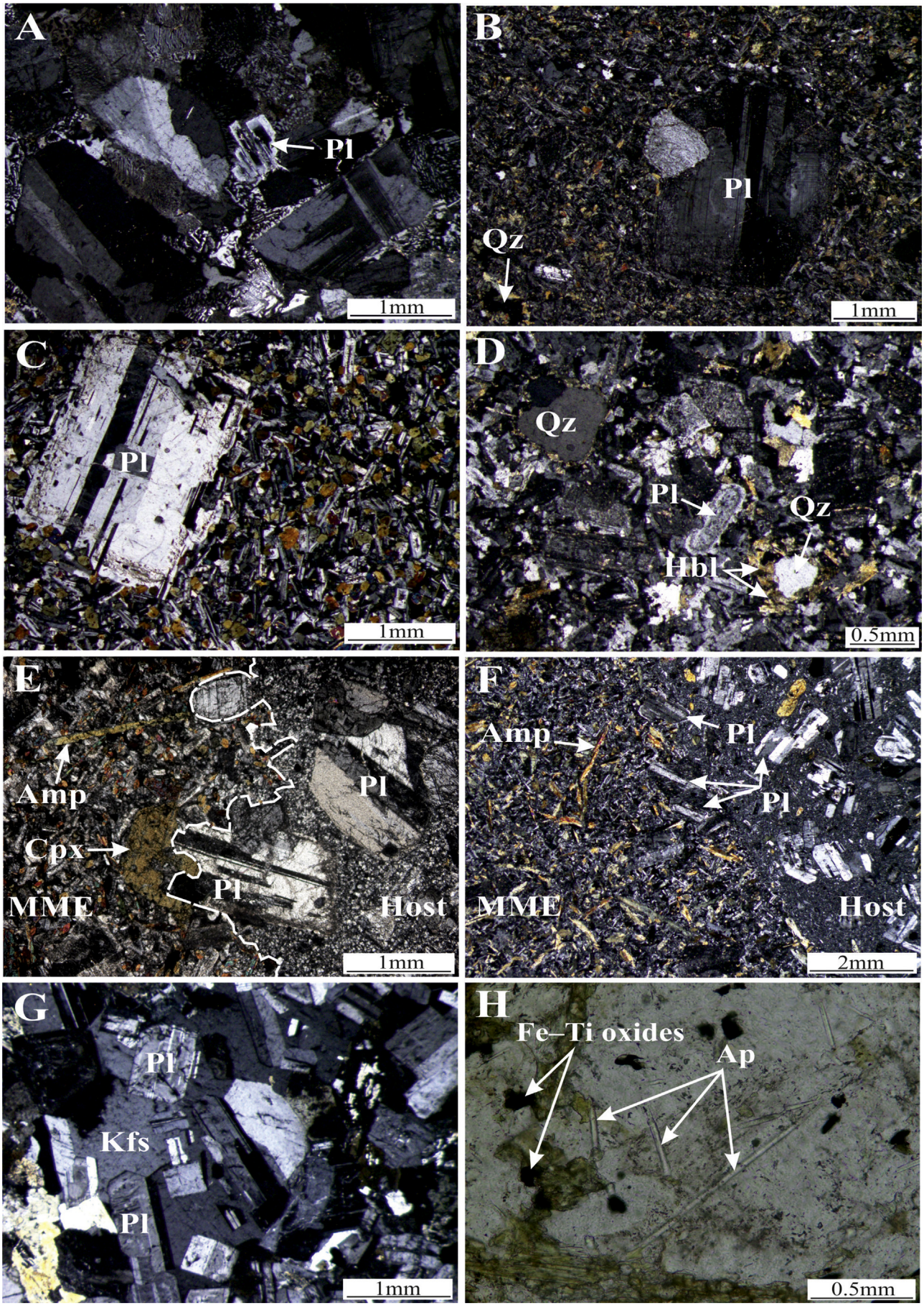
A
Pl
1mm
B
Pl
Qz
1mm
C
Pl
1mm
D
Qz
Pl
Qz
Hbl
0.5mm
E
Amp
Pl
Cpx
Pl
MME
Host
1mm
F
Amp
Pl
Pl
MME
Host
2mm
G
Pl
Kfs
Pl
1mm
H
Fe–Ti oxides
Ap
0.5mm

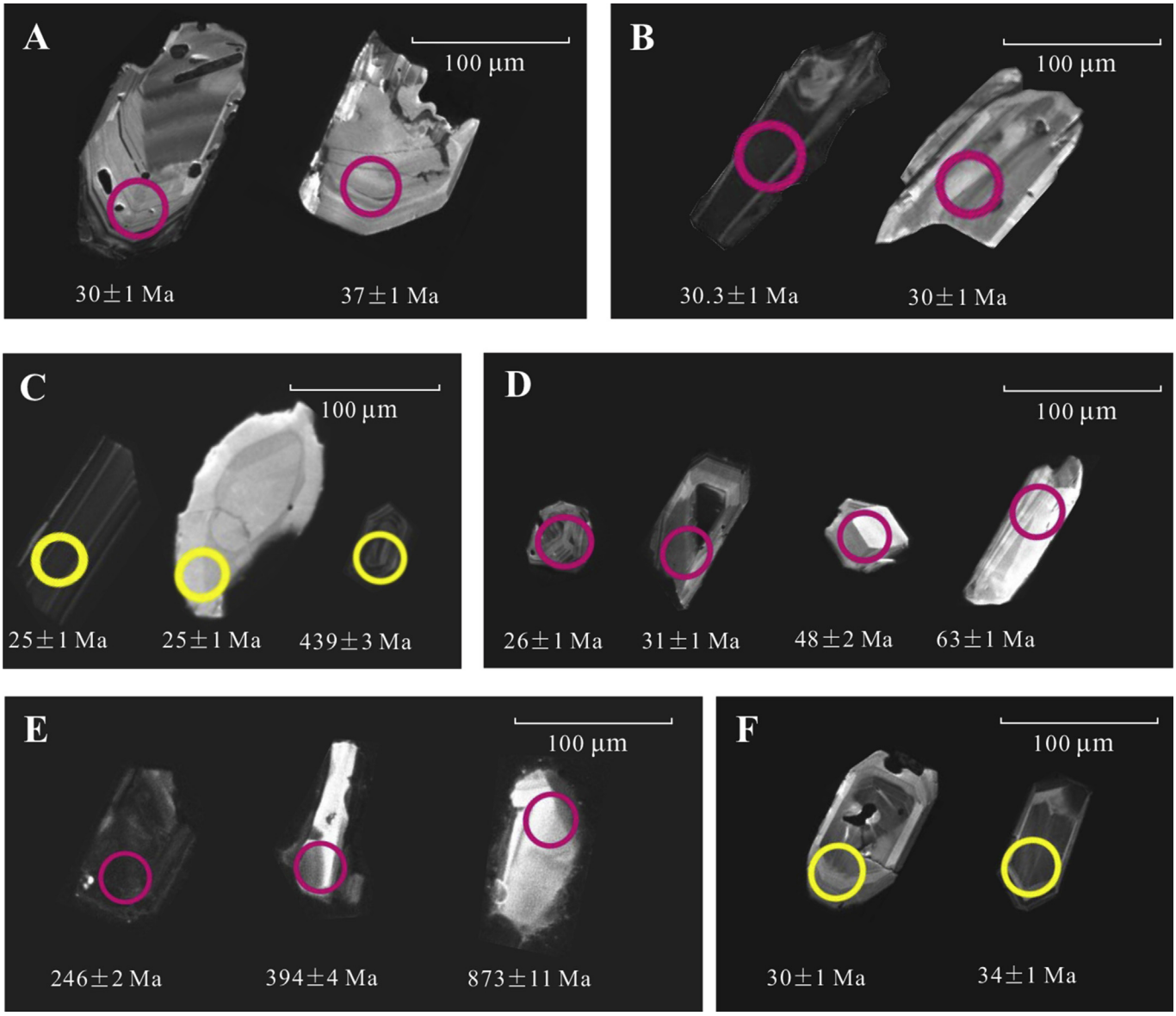

Figure 6. (A–F) CL images of some representative zircon crystals used for U-Pb dating by LA-ICP-MS from the (A) monzodiorite (C-15-8); (B) diorite (C-15-7); (C) diorite (C-15-9); (D) gabbroic diorite (C-15-10); (E) diorite (C-15-11) and (F) granite (C-15-1). Note that some contain inherited cores. The circles are analysis spots marked with ages.

suggest significant fractionations for some mafic and felsic phases during magma evolution. The host rocks have chemical composition slightly different than those of the MMEs, with lower CaO, MgO, Fe_2O_3, P_2O_5, TiO_2, MnO and Al_2O_3, and higher K_2O and Na_2O. Similarly, the MMEs show higher Co, Sr, Y, and lower Ba, Th, Rb than their respective host rocks (Supplementary Table 2 and Fig. 10), although Nb and Nd contents are nearly similar. Chondrite-normalized REE patterns are plotted in Fig. 11A and B. The REE abundance patterns of the samples are all characterized by a fractionation between light and heavy REEs. All the samples exhibit similar trace element abundance patterns, with enrichment in LILEs (e.g. Cs, Rb, Th, K, Ba, U and Sr) and strongly-pronounced depletion in HFSEs, such as Ti, P and Nb compared to the primitive mantle (Fig. 11C and D).

The early Oligocene granitic host rocks display a more fractionated REE pattern ($(La/Yb)_{CN}$ = 8.54–14.03 and $(Gd/Yb)_{CN}$ = 1.26–1.42; Supplementary Table 2), with heavy flatter REE patterns than their mafic enclaves ($(La/Yb)_{CN}$ = 2.29–2.56 and $(Gd/Yb)_{CN}$ = 0.86–1.06) (Supplementary Table 2 and Fig. 11A). These ratios in two samples of the gabbroic diorite enclaves are ($(La/Yb)_{CN}$ = 7.89–8.38 and $(Gd/Yb)_{CN}$ = 1.91–2.02) (Supplementary Table 2 and Fig. 11B). Chondrite-normalized REE patterns for other samples are moderately fractionated and relatively flat ($(La/Yb)_{CN}$ = 2.52–5.49 and $(Gd/Yb)_{CN}$ = 1.07–1.59) (Supplementary Table 2 and Fig. 11A and B). Most of the samples show small Eu depletion (Eu/Eu^* = 0.32–0.97, Supplementary Table 2 and Fig. 9F), except for a few which show no significant Eu anomalies (Eu/Eu^* = 1.02–1.1). The relative depletion of Eu probably resulted from

Figure 5. (A–G) Photomicrographs showing textural relationships of the host granitoid rocks and their enclaves. All the microphotographs are shown in crossed polarized light (XPL). (H) Abundant acicular apatite and Fe–Ti oxides enclosed in plagioclase (in MMEs, seen under plane-polarized light: PPL). The features are amphibole (Amp), clinopyroxene (Cpx), plagioclase (Pl), quartz (Qz), apatite (Ap), K-feldspar (Kfs) and hornblende (Hbl).

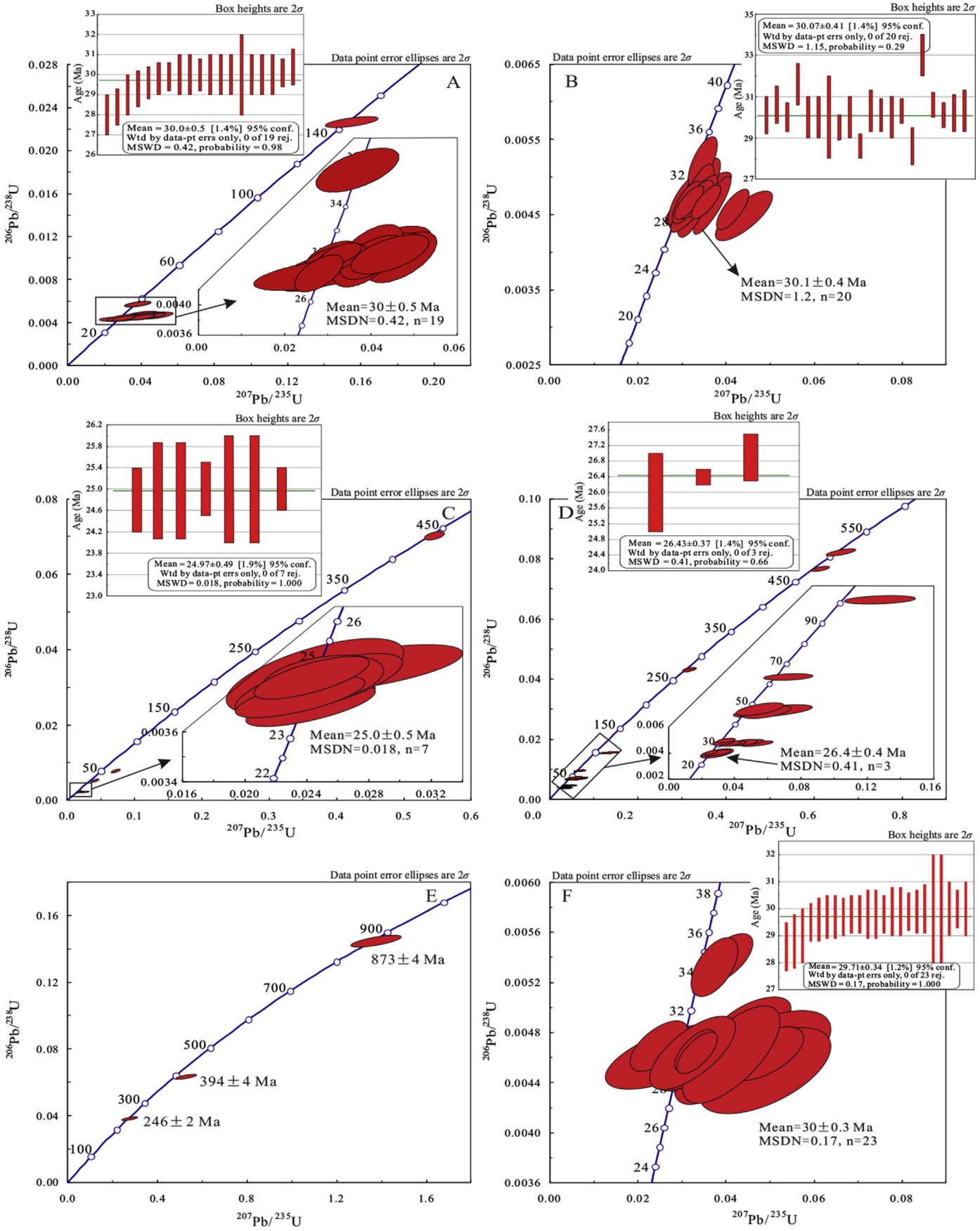

Figure 7. (A–F) Zircon U–Pb concordia diagram for representative samples of the NPC; (A) monzodiorite (C-15-8); (B) diorite (C-15-7); (C) diorite (C-15-9); (D) gabbroic diorite (C-15-10); (E) diorite (C-15-11) and (F) granite (C-15-1).

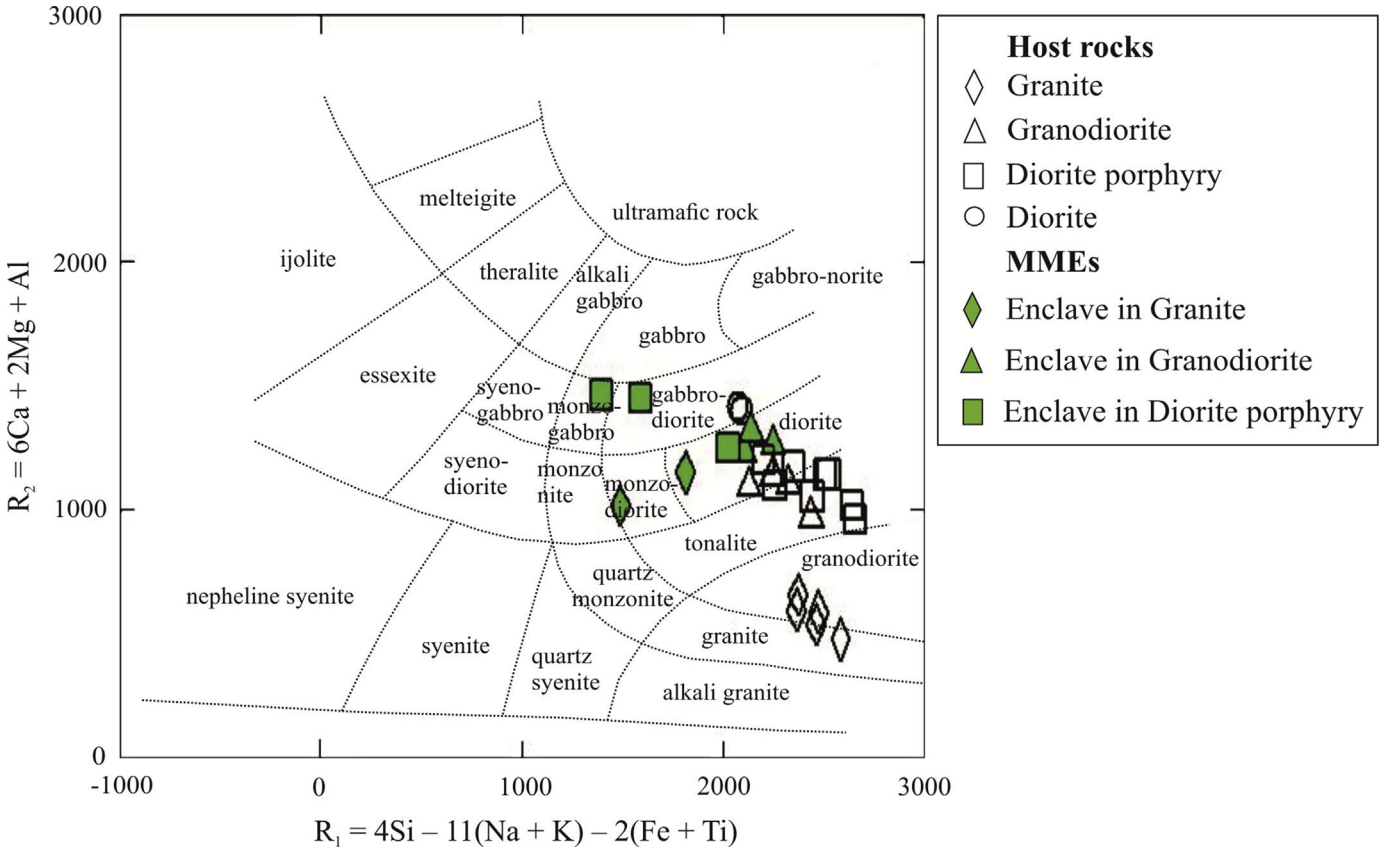

Figure 8. Classification diagram (De la Roche et al., 1980) for the Nodoushan Plutonic Complex.

the fractional crystallization of plagioclase during magma evolution. Accordingly, the Oligocene Nodoushan intrusions show relatively low La/Yb ratios (3.43–21.04), relative depletion of Eu ($Eu/Eu^*<1$), and less-fractionated heavy REE (Sm/Yb = 0.98–2.60; Gd/Yb = 1.07–2.53), which reflects plagioclase and pyroxene fractionation from the melt, is seen in most arc magmatic rocks (Fig. 14D).

The early Oligocene dioritic magma is enriched in middle rare earth elements ($MREE_S$; Sm-Ho) and HREE, and depleted in LREE relative to the granitic magma (early Oligocene host rocks, Fig. 11A). In addition, Harker diagrams relating to these intrusions (Fig. 10), indicate that there is a certain gap between the two units mentioned; which implies that they have different origins. In the granitic intrusions, despite similar mineralogy and isotopic characteristics (Fig. 12) the MMEs show some variety in chemical composition, especially in trace and rare earth elements (Fig. 11A and C). They have dioritic to monzodioritic compositions and show geochemical features in the range between their granitic host and dioritic samples. The HREE contents of these MMEs are higher than their host rocks and show a significant geochemical similarity to the dioritic intrusions; which are coeval with their granitic host rocks, i.e. early Oligocene (Fig. 11A). Furthermore, on the Harker variation diagrams; these enclaves mostly lie between their granitic host rocks and dioritic samples (Fig. 10). Comparison of mineralogy, geochemistry and isotopic features of dioritic and granitic intrusions suggest that the isotopic and thermal interaction of the mafic magma with them was the same; and that it was the main process during formation of the MMEs in the lower Oligocene. The chondrite-normalized REE patterns (Sun and McDonough, 1989) of the early Oligocene granitic host rocks show enrichment in LREEs; their mafic enclaves are enriched in HREEs and MREEs (Fig. 11A) but show significant relative depletion of Eu (Eu/Eu^* = 0.32–0.47; Fig. 9F) relative to the granitic host rocks (Eu/Eu^* = 0.82–1.1). In the primitive mantle-normalized trace element variation diagram (Sun and McDonough, 1989), the granitic host rocks exhibit similar trace element abundance patterns, with enrichments in LILEs (e.g. Cs, Rb, Th, K, Ba) and pronounced relative depletion in HFSEs (e.g. Ti, Nb, Ta, P) relative to the primitive mantle (Fig. 11C). Nevertheless, their mafic enclaves show markedly higher HREEs, and Ti, P, Nb and Y contents than their granitic host rocks.

Barbarin and Didier (1992) suggested that various types of enclaves are produced by the injection of mafic magma into granitoid magma at different stages of crystallization. Thus, the Nodoushan MMEs may be divided into two groups with respect to their REE chemical features. The first group exhibits a greater similarity to their host while the second group has higher HREE contents than their host rocks. The first group of MMEs display more fractionated REE pattern (host rocks and Group 1 MME: $(La/Yb)_{CN}$ = 2.52–8.38; Group 2 MMEs and diorite: $(La/Yb)_{CN}$ = 2.29–4.65) with a smaller Eu anomaly compared with the second group of enclaves and diorite (host rocks and Group 1 MMEs: Eu/Eu^* = 0.82–1.04; Group 2 MMEs and diorite: Eu/Eu^* = 0.32–0.78) (Supplementary Table 2 and Fig. 9F).

4.4. Sr and Nd isotopic composition

Representative samples for Sr and Nd isotopic analysis given in Table 3, were chosen in a way that encompass the broad compositional spectrum of the host rocks and mafic enclaves, that is, from the most primitive rock types to the most evolved ones. Initial Nd and Sr isotopic compositions were calculated at the age of 30.52 Ma and 30.06 Ma for diorite and granite units, respectively. Initial isotopic compositions were also calculated at 24.994 Ma for the

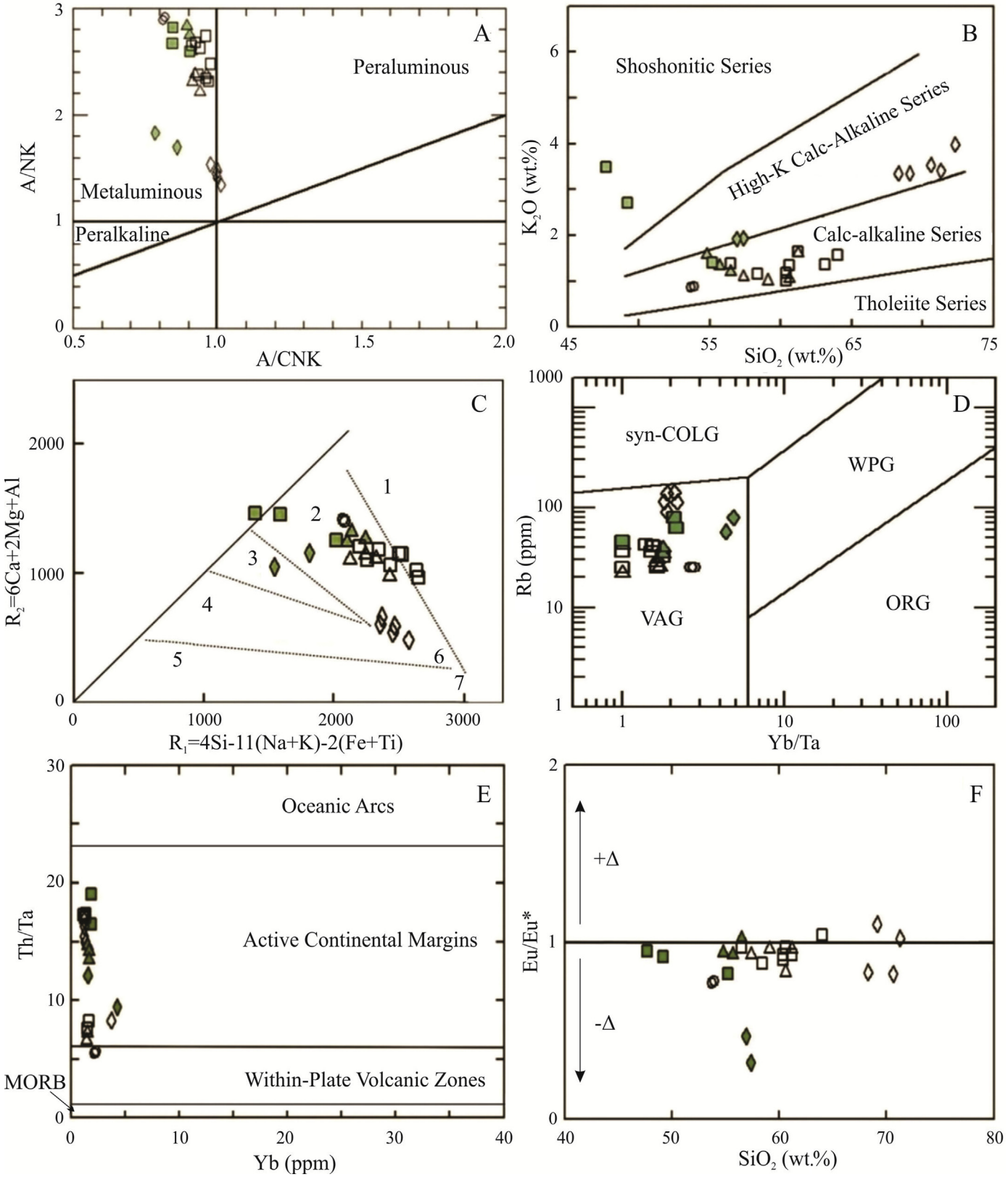

Figure 9. Chemical variation diagrams for the Nodoushan plutons illustrating some chemical features that help distinguish between the granitoid rocks. (A) A/NK (molar $Al_2O_3/Na_2O + K_2O$) versus A/CNK (molar $Al_2O_3/CaO + Na_2O + K_2O$) (after Maniar and Piccoli, 1989) diagram for the plutons. (B) K_2O versus SiO_2 diagram for the samples with lines separating tholoiitic, calc-alkaline, high-K calc-alkaline and shoshonitic series of Peccerillo and Taylor (1976). (C) Plots of Nodoushan Plutonic Complex samples on R_1–R_2 diagram (De la Roche et al., 1980). Fields are numbered according to Batchelor and Bowden (1985): 1 – mantle fractionates, 2 – pre-plate collision suites, 3 – post-collision suites, 4 – late orogenic magmas, 5 – anorogenic suites, 6 – syn-collisional (anatectic) suites, 7 – post-orogenic. The Nodoushan samples fall into the pre-plate collision field. $R_1 = 4Si - 11(Na + K) - 2(Fe + Ti)$ and $R_2 = 6Ca + 2\,Mg + Al$. (D) Tectonic discrimination diagram showing Rb versus Yb/Ta from Pearce et al. (1984). Fields for Syn-COLG (syn-collisional), VAG (volcanic arc), WPG (within-plate) and ORG (ocean-ridge) granites are indicated. (E) Diagram showing Yb versus Th/Ta, field boundary is from Schandl and Gorton (2002). (F) SiO_2 vs. Eu/Eu* ($Eu/Eu^* = Eu_{CN}/[(Sm_{CN} + Gd_{CN})/2]$). Positive Eu anomalies (+Δ) are consistent with hydrous and oxidized nature of magmas. Base diagram and boundaries of Eu anomaly are from Richards et al. (2001). Symbols are the same as in Fig. 3.

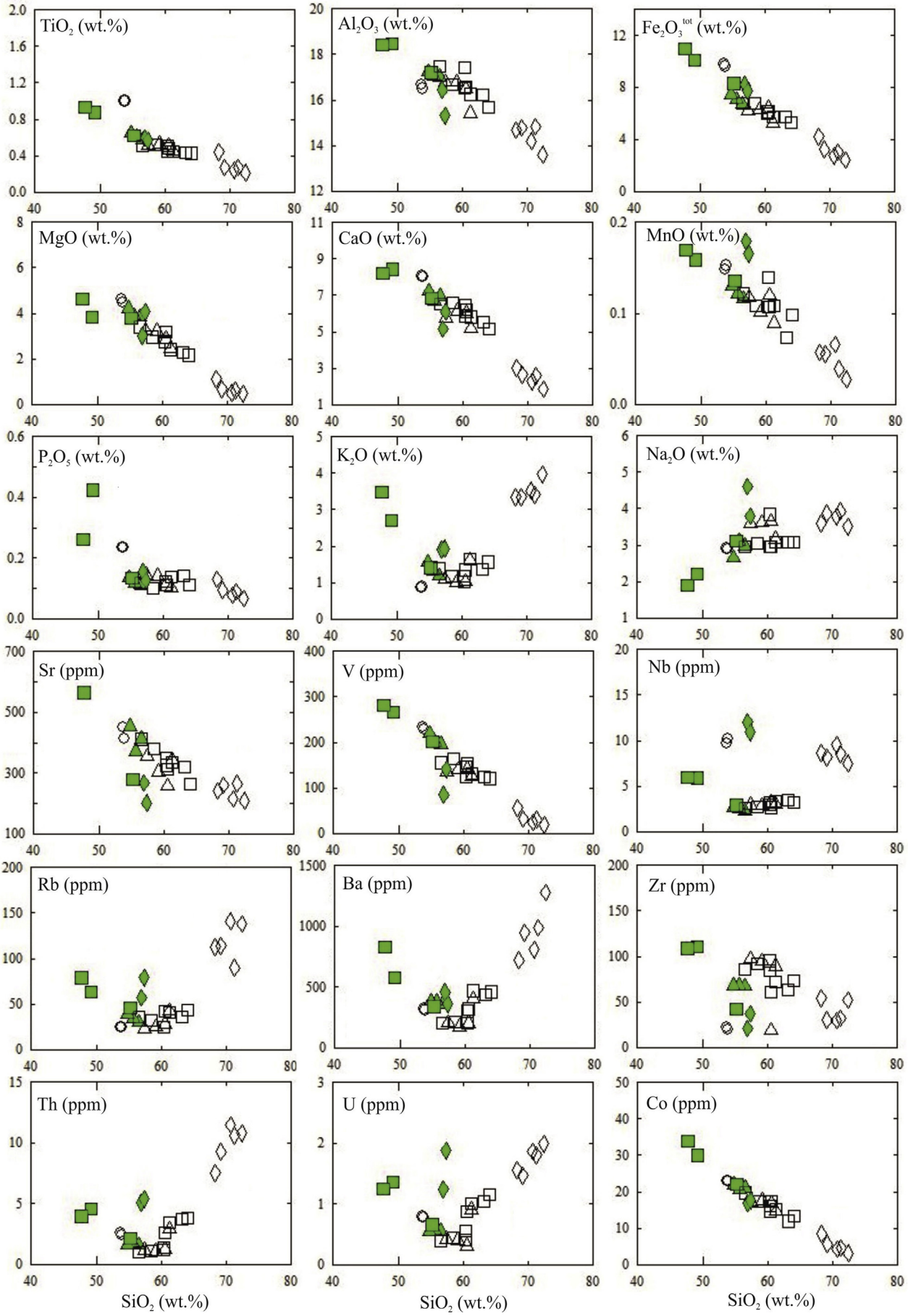

Figure 10. Harker variation diagrams for samples from the plutons. Symbols are the same as in Fig. 3.

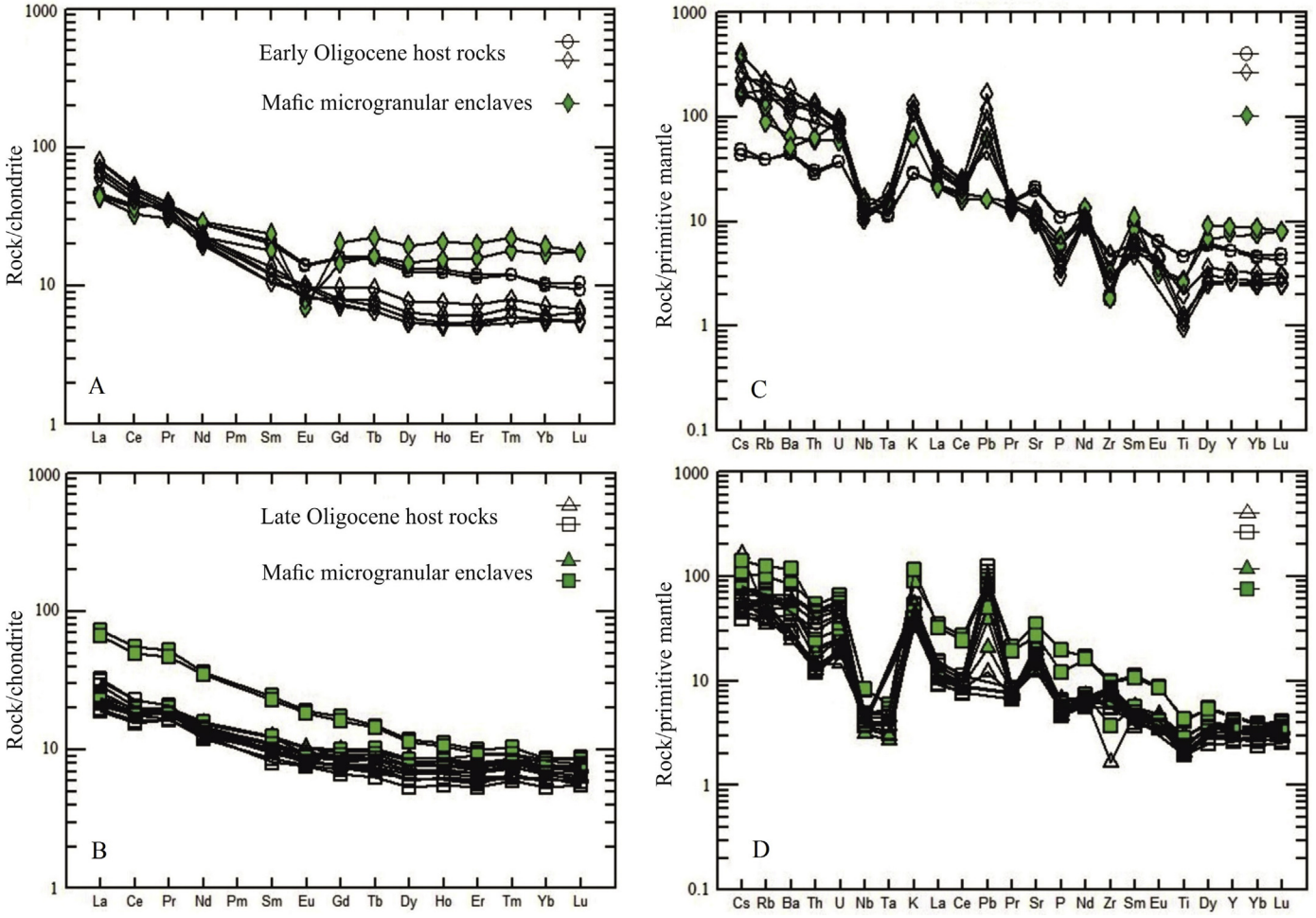

Figure 11. (A–B) Chondrite-normalized (to values given in Nakamura, 1974) REE abundance patterns and (C–D) primitive mantle-normalized multi-element variation patterns (normalized to values given in Sun and McDonough, 1989) for the selected samples from the Nodoushan Plutonic Complex.

granodiorite and 24.13 Ma for the diorite porphyry intrusions (obtained via zircon U–Pb geochronology, Shahsavari Alavijeh et al., 2017).

Regardless of rock types and SiO_2 content, the host rocks of the NPC display relatively homogeneous isotopic compositions of I_{Sr} ranging from 0.705045–0.707959 and of $\varepsilon_{Nd}(t)$ from −3.23 to +3.80. The corresponding Nd model ages (T_{DM}) are in the range of 0.58–1.37 Ga. The isotopic compositions of $^{87}Sr/^{86}Sr$ ratios range from 0.705167 to 0.708538 and $^{143}Nd/^{144}Nd$ ratios range from 0.512463 to 0.512826; and $\varepsilon_{Nd}(0) = -3.41$ to 3.67. Compared with the host rocks, the MMEs are relatively homogeneous in isotopic composition, with I_{Sr} ranging from 0.705513 to 0.707275 and $\varepsilon_{Nd}(t)$ from −1.46 to 4.62. The MMEs have T_{DM} ranging from 0.49 Ga to 1.39 Ga. They show the measured $^{87}Sr/^{86}Sr$ ratios $(^{87}Sr/^{86}Sr)_m$ range from 0.705665 to 0.707761 and $(^{143}Nd/^{144}Nd)_m$ = 0.512556–0.512868, similar to their respective host rocks and $\varepsilon_{Nd}(0) = -1.60$ to 4.49.

In order to reveal their source properties, we plot the initial $^{143}Nd/^{144}Nd$ ratios (expressed as $\varepsilon_{Nd}(t)$ values) against I_{Sr} (Fig. 12A). All samples show high initial Sr and intermediate initial $^{143}Nd/^{144}Nd$ values, following the trend of lower continental crust (LCC) and away from the trend of upper continental crust (UCC); the NPC samples lie near the fields of enriched mantle II (EMII). The variations in the $^{87}Sr/^{86}Sr$ and $^{143}Nd/^{144}Nd$ ratios of the NPC host rocks and MMEs are shown and compared with bulk earth and the mantle array in Fig. 12B. All samples plot to the right of the mantle array in Fig. 12A and B, and show a negative correlation between both parameters. Such a correlation is universally attributed to magma interaction between crustal and mantle sources (e.g. Rollinson, 1993; Parada et al., 1999; Chen et al., 2002).

5. Discussion

5.1. Universal considerations and hypothetical genetic model

As main components of the continental crust, granitoids are regarded as a key element to understand tectonics and geological evolution. On the other hand, subduction and collision-related regions are undoubtedly the most complex tectonic provinces on Earth (Wilson, 1989). Most granitoids have been geochemically modified, not only by partial melting in their source area and fractional crystallization during the ascension and emplacement of magma, but also by open system processes like assimilation and magma mingling/mixing. In such settings, therefore, granitoids display variable field, petrographic, mineralogical and geochemical features. They are genetically classified as peraluminous granitoids of crustal origin (e.g. Chappell and White, 1992; Chappell, 1999), alkaline granitoids of mantle origin (e.g. Turner et al., 1992; Han et al., 1997; Volkert et al., 2000) and calc-alkaline granitoids of

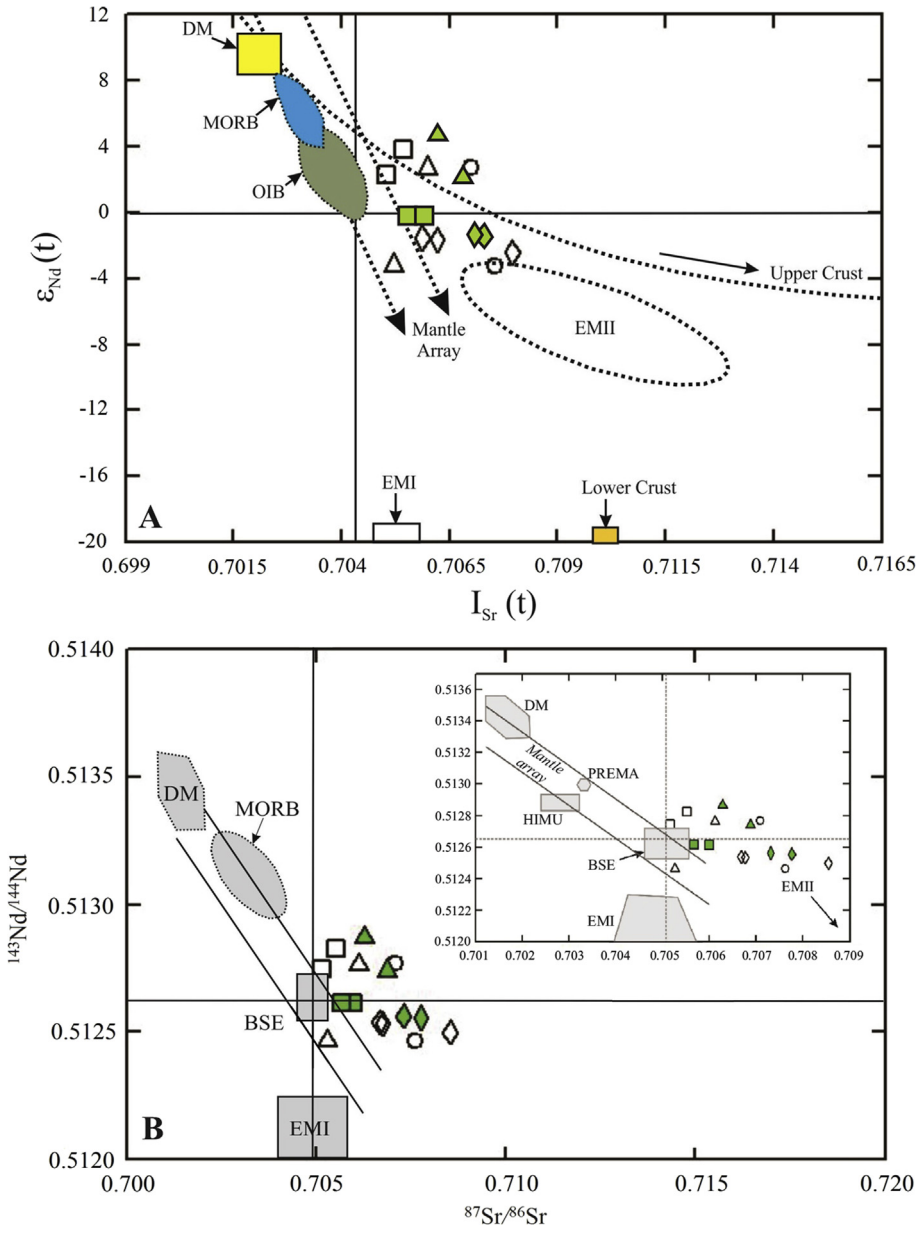

Figure 12. (A) Plot of $I_{Sr}(t)$ versus $\varepsilon_{Nd}(t)$ values. MORB: mid-ocean ridge basalt; DM: depleted mantle; OIB: ocean-island basalt after Zindler and Hart (1986); EMI and EMII represent two types of mantle end-members, respectively (Hou et al., 2011). The reference of the lower crust values is from Ben Othman et al. (1984). (B) $^{143}Nd/^{144}Nd$ and $^{87}Sr/^{86}Sr$ isotopic initial ratios for representative rocks of the NPC. Shaded area shows the main oceanic mantle reservoirs of Zindler and Hart (1986). EMI and EMII, enriched mantle; DM, depleted mantle; BSE, bulk silicate Earth; HIMU, mantle with high U/Pb ratio; PREMA, frequently observed prevalent mantle composition. Symbols are the same as in Fig. 3.

mixed origin, having various proportions of crust- and mantle-derived components (e.g. Poli and Tommasini, 1991; Barbarin and Didier, 1992; Wiebe, 1996; Altherr et al., 1999; Chen et al., 2002).

An important part of the overall processes in calc-alkaline magmatism is the mafic–felsic interaction, as manifested by rheological and geochemical data of coeval magmas (e.g. Barbarin and Didier, 1992; Wiebe, 1996; Karslı et al., 2007), where the mafic components are shown by those MMEs within the host rocks (e.g. Vernon, 1990; Poli and Tommasini, 1991; Barbarin and Didier, 1992; Elburg, 1996). The hybrid host rocks from the NPC have a wide range of silica content (SiO_2 = 57–72 wt.%, except for the diorite samples with SiO_2 = 54 wt.%) and relatively high Mg# (26–51). It seems unlikely that felsic magmas were derived from a basaltic parent magma by assimilation–fractional crystallization (AFC) or fractional crystallization processes, as suggested by Grove and Donnelly-Nolan (1986) and Han et al. (1997), because the host rocks have SiO_2 content >54 wt.%, and none of the rocks in the region are of basaltic composition. In other words, if the latter process occurred during the generation of the felsic rocks, then the basic rocks would be much more abundant than the felsic. Such felsic magmas (SiO_2 = 54–72 wt.%; Mg# = 26–51) cannot be produced by the differentiation of mantle-derived mafic magmas. In addition, Sr–Nd isotopes alone cannot be considered to classify them as mantle-derived mafic magmas; some involvement of crustal melts in the source are essential. The MMEs of the plutons are also characterized by relatively low silica content (48%–57%, average 54%) and relatively high Mg# (42.15–53.04), and therefore could not originate from the partial melting of the lower crust. The Mg# values would be very low in the samples if the granitoid magmas were derived from the partial melting of such isotopically

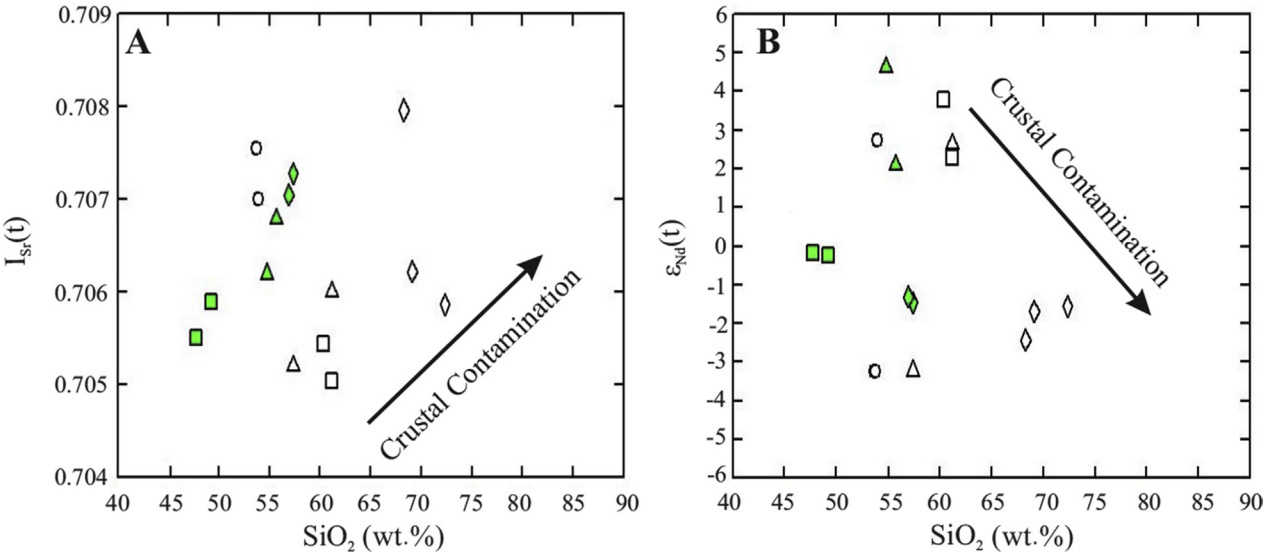

Figure 13. (A–B) Silica versus $I_{Sr}(t)$ and $\varepsilon_{Nd}(t)$ plots for the samples from the plutons. Symbols are the same as in Fig. 3.

similar crustal rocks. Consequently, a mantle contribution is required in their genesis. Furthermore, high-K magmas were construed to originate from a mixture between mantle magma and crustal melts (e.g. Ferré and Leake, 2001) or a metasomatized mantle source (e.g. Soesoo, 2000). The I_{Sr} (30.06 Ma) ratios (>0.705) are not compatible with the mantle derivation for high-K magmas.

We suggest a magma interaction model for the origin of the NPC. The mantle-derived mafic magma intrusion into the lower continental crust, which provides the necessary heat source for the dehydration melting of the lower crust, produces the granitoid melt (e.g. Rushmer, 1991; Rapp and Watson, 1995; Petford and Gallagher, 2001). Many authors also propose that mantle-derived mafic magmas play a basic role in the genesis of felsic magmas by both heat and material transfer to the magma source in the crust (Huppert and Sparks, 1988; Dias and Leterrier, 1994). López and Castro (2001), Wolf and Wyllie (1994) and Wyllie and Wolf (1993) experimentally indicated that amphibolites start to melt at relatively high temperatures (800–900 °C) at pressures <1 GPa, whilst dehydration melting commences at temperatures as low as 750 °C, at ~1 GPa. Moreover, the melt composition created by the partial melting of the mafic lower crust are controlled by the degree and P–T conditions of the melting, source composition and water content (e.g. Rapp et al., 1991; Şen and Dunn, 1994; Wolf and Wyllie, 1994; Rapp and Watson, 1995; Winther, 1996; López and Castro, 2001). Recent experimental data suggest that the partial melting of the mafic lower crust could produce melts of metaluminous granitoid composition irrespective of the degree of the partial melting (e.g. Rushmer, 1991; Roberts and Clemens, 1993; Tepper et al., 1993; Wolf and Wyllie, 1994; Rapp and Watson, 1995). Experiments performed by Rapp and Watson (1995) display less silicic melts derived from high degrees of partial melting in the lower crust.

Subsequently, interaction between a granitoidic melt and mantle-derived mafic magma lead to a hybrid parental magma that underwent a fractional crystallization process en route to higher crustal levels, producing a wide variety of granitoidic rocks in the area. The interaction process is plainly supported by inversely correlated parameters in Fig. 12A and B; most of the samples plot between crust and mantle components. Interestingly, the analytical uncertainty for ε_{Nd} is less than 0.5 units. Therefore, the range of variation over 2 units of ε_{Nd} shown by these samples most likely show a hybridization of two magmas with different isotopic compositions.

5.2. Fractional crystallization

An acceptable mechanism to explain the generation of a wide variety of rock types is fractional crystallization. Major- and trace-element variation trends indicate that fractional crystallization probably played a dominant role in the evolution of these rocks (Fig. 10). However, it is clear that the host rocks and MMEs have different origins. The decrease in Al_2O_3, CaO, MgO, Fe_2O_3, TiO_2, P_2O_5, Sr, and increase in K_2O and Rb with the increase of SiO_2 are related to the fractionation of plagioclase, hornblende, apatite, titanite and Fe–Ti oxide. The negative CaO, Fe_2O_3 and MgO correlations with SiO_2 may also reflect in the fractionation of pyroxene. The LILE, Ba and Rb show a fairly linear positive correlation, whiles Sr exhibits an apparent declination with increasing SiO_2, reflecting the removal of plagioclase. Negative Eu anomalies and a decrease of Sr with increasing silica indicate that plagioclase was an important fractionating phase. In addition, the fractionation of accessory phases such as zircon and titanite is registered by the depletion in zirconium and yttrium. These geochemical characteristics along with their mineralogy are in accordance with a genetic relationship between the least and most evolved products of the plutons.

Despite the fact that fractional crystallization is considered as one of the dominant processes, the whole-rock and Nd–Sr isotopic data suggest that a small amount of assimilation/contamination plays some role in the genesis of these hybrid rocks. The assimilation effects may be evaluated by elemental and isotopic ratios. The AFC process is supported by the trend of the granitoid samples in the Ce/Yb–Ce plot which show decreasing Ce/Yb ratios with decreasing Ce (Fig. 14A). During the AFC process, the most contaminated samples are the most fractionated ones, i.e. when a group of rocks is associated with this process, we expect to see a positive correlation between SiO_2 and initial Sr ratios. There does not seem to be a strong relationship between $(^{87}Sr/^{86}Sr)_i$ or $\varepsilon_{Nd}(t)$ and SiO_2 contents (Fig. 13A and B) as one would expect if the crustal assimilation is a predominant petrogenetic process. However, a plot of $(^{87}Sr/^{86}Sr)_i$ versus SiO_2 (Fig. 13A) shows a minor amount of

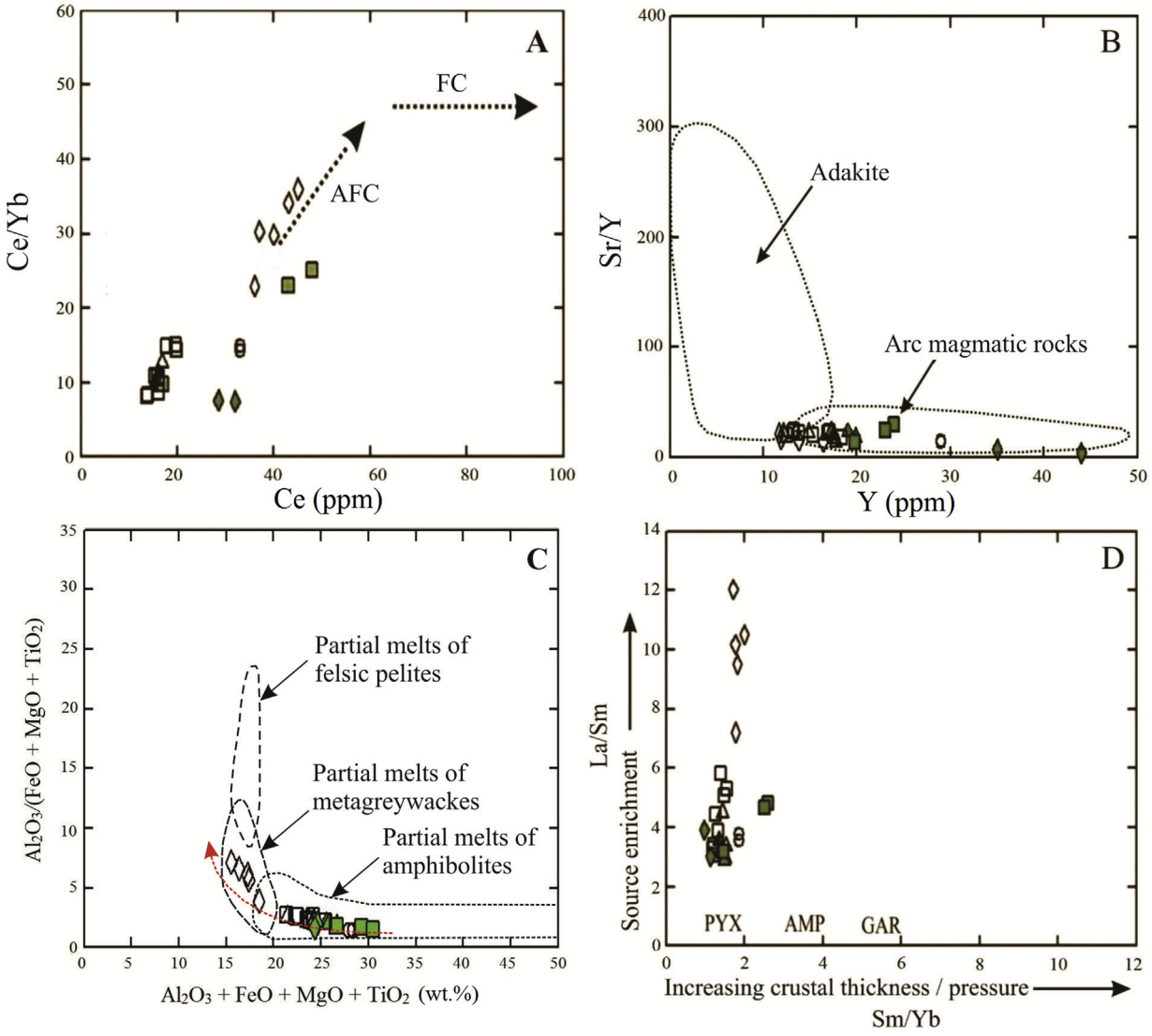

Figure 14. (A) Variation diagram of Ce/Yb versus Ce of the Nodoushan Plutonic Complex (Ajaji et al., 1998). AFC: assimilation-fractional crystallization; FC: fractional crystallization. (B) Sr/Y versus Y (Defant and Drummond, 1990) for discrimination between adakites and normal calc-alkaline rocks. (C) Compositions of the Nodoushan rocks in comparison to compositional fields of experimentally derived partial melts of metapelites, metagreywackes and amphibolites. Data for experimentally derived liquids from Patino-Douce (1999). (D) Sm/Yb vs. La/Sm ratios as discriminants for changing pressure in the source mineralogy and source enrichment. Abbreviations used: PYX—pyroxene, AMP—amphibole, GAR—garnet. Base diagram and boundaries of residual minerals from Kay and Mpodozis (2001). Symbols are the same as in Fig. 3.

crustal contamination, which is not a predominant petrogenetic process, in combination with the effects of fractional crystallization during the emplacement of the hybrid magma in the crust.

5.3. Origin of microgranular enclaves: restite, cognate or mixing?

There are many discussions regarding magmatic versus non-magmatic origins of the MMEs. The restite hypothesis considers the origin of microgranular enclaves as refractory solid residues of partial melting from the source region (e.g. Vernon, 1983; Chappell and White, 1991; Collins, 1998; White et al., 1999). Restite enclaves are often enclosed in S-type granitoids; they are characterized with Al-rich minerals (such as sillimanite, garnet, etc.) and clear metamorphic textures. Petrological characteristics of restite enclaves display that they can result from the melting of crustal rocks, and that the geochemistry of enclaves and host rocks should be supplementary. However, mineralogical and geochemical characteristics of the NPC MMEs are not in accordance with restite components. The studied MMEs contain neither garnet, cordierite, sillimanite, and alusite nor residual minerals formed from mica dehydration. Moreover, oscillatory zoning, poikilitic and interstitial igneous textures are the main features that indicate magmatic crystallization (Vernon, 1983; Didier, 1984).

Magmatic microgranular enclaves are particularly abundant in continental margin and island arc batholiths (Didier, 1973; Didier and Barbarin, 1991). Although, the microgranular enclaves represent only about 1–2 vol.% of granitoid plutons (Link, 1969), studying such inclusions is a valuable tool to understand the melt-source rocks and subsequent evolution of granitoid bodies. In host rocks, they are commonly interpreted as products of mixing and mingling of mantle- and crust-derived magmas (Castro et al., 1990; Dorais et al., 1990; Vernon, 1991, 1983; Barbarin and Didier, 1992). Nonetheless, their origin is still controversial. Further, the magmatic interaction process has become the most prevalent model to interpret the origin of the MMEs. Meanwhile, their finer grain sizes are being attributed to the undercooling of a mafic magma in a cooler, felsic magma (e.g. Vernon, 1984; Wiebe, 1991; Barbarin and Didier, 1992; Perugini and Poli, 2000; Kumar et al., 2004; Karslı

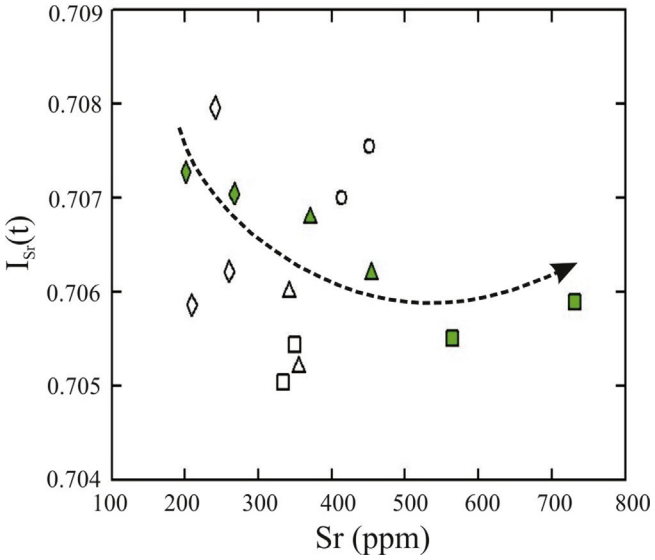

Figure 15. $I_{Sr}(t)$ versus Sr (ppm) plot for the samples from the Nodoushan Plutonic Complex. Symbols are the same as in Fig. 3.

et al., 2007). The mineral assemblages, chemical relationships and isotopic compositions in the MMEs from the NPC are similar to their host rocks. The similarities of Sr–Nd isotopic compositions in particular reflect the fact that the MMEs are not solid residues of partial melting that represent a restitic origin. This actually coincides with both cognate and mixed origins. The MMEs from the Los Pedroshes granodiorite have similar isotopic compositions with their host rocks, indicating they formed from a coeval, cognate magma (Donaire et al., 2005). Also in the MMEs, the occurrences of both diffuse and rounded contacts indicate that magmatic batches with variable viscosity existed in the same magmatic system (e.g. Nittmann et al., 1985; Perugini et al., 2004). Additionally, the presence of these contacts between the MMEs and their host rocks points out that both processes of quenching of mafic and felsic magmas heated by a mafic magma played important roles in the generation of the MMEs in the dynamic magma chamber. Furthermore, isotopic equilibrium has been attained between the mafic enclaves and their host by the passage of time (e.g. Poli and Tommasini, 1991). Many researchers have announced partial or complete isotopic equilibration of the MMEs with their host (e.g. Pin et al., 1990; Holden et al., 1991; Elburg, 1996). Some also show that isotopic equilibration progresses faster than chemical equilibration, and Sr isotopic equilibrium is faster than that of Nd (e.g. Holden et al., 1987; Pin et al., 1990). Compared with the isotopic

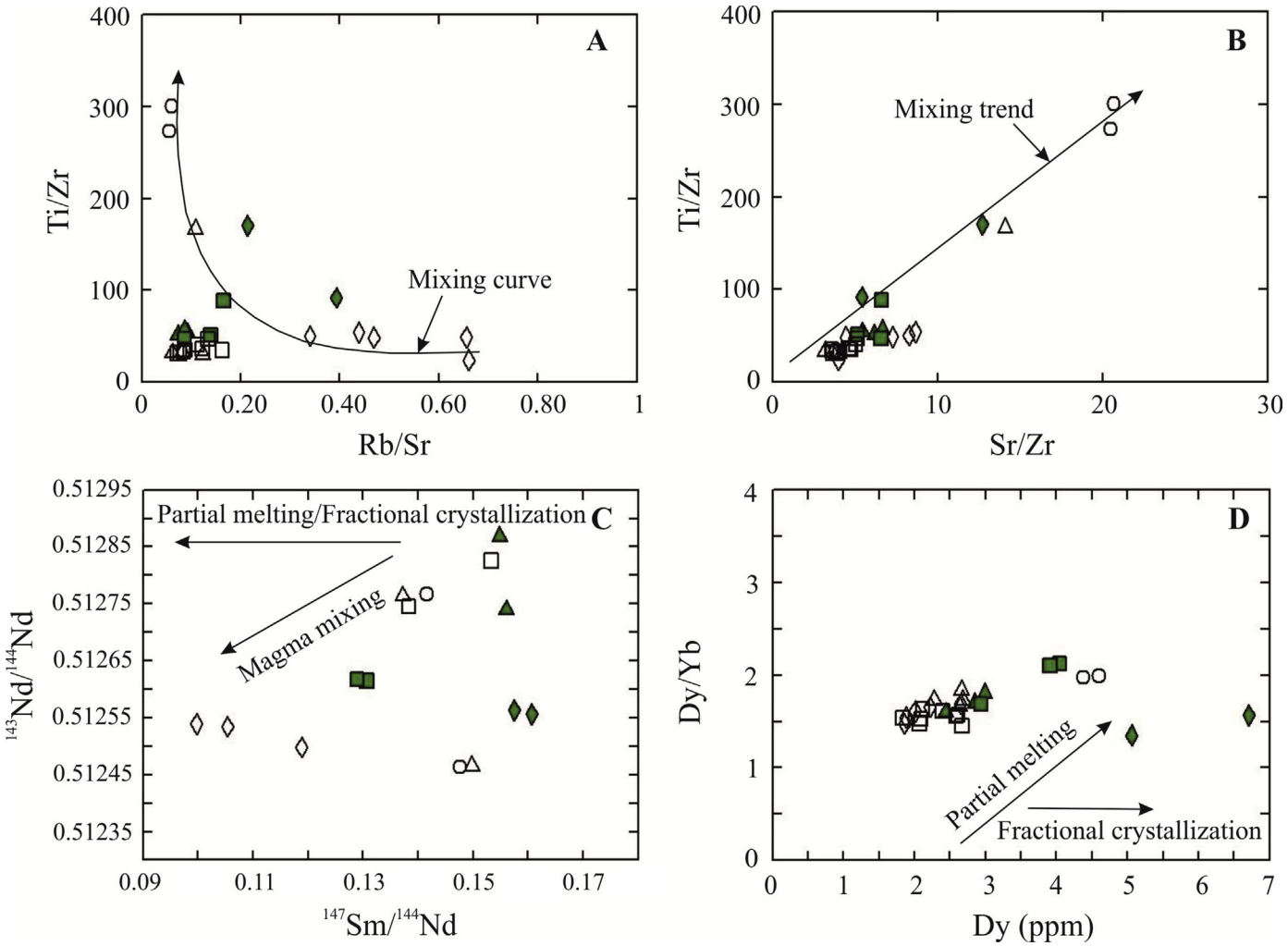

Figure 16. (A–B) Inter element ratio plots, (C) $^{143}Nd/^{144}Nd$ versus $^{147}Sm/^{144}Nd$ diagram, (D) Dy/Yb versus Dy contents (Gao et al., 2007) for the Nodoushan Plutonic Complex. Symbols are the same as in Fig. 3.

composition of Nd, the Sr of the host and the enclaves are more likely to be equilibrated through diffusion exchange. From the data in Table 3, the sample N129E^{+} (MME) exhibits very similar isotopic composition of $I_{Sr}(t)$ (0.705513) with respect to the host rock (N34 = 0.705448), while their $^{143}Nd/^{144}Nd$ ratios are slightly different. This strong isotopic similarity could be construed as having undergone a more or less complete isotopic equilibrium process. However, in the MMEs and their host rocks, the abundances of major and trace elements are slightly different (Supplementary Table 2). Both represent comparable variations without a chemical gap in most diagrams (Figs. 9 and 10). Such a chemical variation is construed in terms of a two-end-member interaction as the fundamental process for the genesis of enclaves and their hybrid host rocks (e.g. Barbarin and Didier, 1992; Wiebe et al., 1997; Perugini et al., 2003). Angular, ellipsoidal or ovoid, rounded and flattened shapes of the MMEs suggest that plastic behavior at the moment of their incorporation into the hybrid host magma are due to their plastic rheology (Frost and Mahood, 1987; Poli and Tommasini, 1991). Additionally, amphibole and biotite contents in the MMEs as mafic phases are always much lower than 50 vol.%. Ferromagnesian phases can nucleate more quickly than feldspar and quartz, and so can be enriched in early crystallization products (Weinberg et al., 2001). Hence, high content of mafic phases in the MMEs are cited as evidence of a cognate process, as proposed by Donaire et al. (2005). The studied MMEs do not seem to agree with the cognate process. Therefore, we deduce that the MMEs must have formed by a magma interaction process, according to their textural and chemical relationships, and similar isotopic compositions between the MMEs and their hybrid host rocks.

5.4. Magma genesis

The continental crust has highly fractionated and enriched LREE, flat HREE, and a positive Pb anomaly, but negative anomalies at Nb–Ta (Taylor and McLennan, 1985). Based on the geochemical data presented above, the samples from the NPC are characterized by pronounced relative depletion of Nb and Ti in spidergrams (Fig. 11C and D), and enriched in LILEs and LREEs, suggesting typical crustal melts. Nonetheless, such features are not always associated with crustal melts, but may reflect the mantle enrichment events prior to melting (Hawkesworth et al., 1993; Rottura et al., 1998). The mafic magma derived from the melting of a chemically enriched SCLM source can lead to the relative enrichment of hybrid host rocks and their MMEs, with initial Sr–Nd ratios. In fact, these features could be inherited from such a mafic magma. The MMEs have relatively low silica content (48%–57%) and relatively high Mg# (42–53), both of which point to an evolved mantle-derived magma. Additionally, diorite porphyry sample N39 characterized by low SiO_2 content (~57 wt.%) and relatively high Mg# (~50) may not have a pure crustal origin (Supplementary Table 2). However, its low Cr (0.98–103 ppm) and Ni (6–20 ppm) content, relative to those of the unfractionated magmas (respectively; >1000 and 200–450), shows that a mafic magma underwent notable fractionation of olivine, pyroxene and spinel prior to the interaction. Moreover, the Al_2O_3 content of the samples (14–18.46 wt.%, mostly >15 wt.%) are not compatible with the basic parent melts in equilibrium with the mantle source (Al_2O_3 <15 wt.%). This is probably due to the fractionation of some Al-poor mafic phases such as orthopyroxene and olivine, which is evidenced by the REE fractionated patterns of the rocks. The weakly negative to slightly positive $\varepsilon_{Nd}(t)$ values (−3.23 to +4.62) and $\varepsilon_{Nd}(0) = -3.41$ to 4.49, slightly depleted $I_{Sr}(t)$ ratios (0.705045–0.707959) and the isotopic compositions of $^{87}Sr/^{86}Sr$ ratios range from 0.705167 to 0.708538, relative enrichments of LREE (e.g. Ce, La) and LILEs (e.g. K, Th, Sr, Ba and Rb) and depletion of HFSEs (e.g. Ti, Nb; pronounced negative anomalies) are all compatible with the melting of a chemically-enriched SCLM, which probably prevailed for the generation of the hybrid rocks.

The SCLM was most likely chemically enriched by fluids (rich in LILEs and LREEs) or melts derived from the dehydration of the down going slab, which contains Cenozoic arc rocks from prior tectonic processes. Therefore, it is likely that the SCLM played a significant role in the genesis of the magmas. This means that the parental magma to the entire spectrum of intermediate rocks is actually a hybrid magma, not a purely mantle-derived basic magma. In association with a more felsic end-member, an upper crust-derived magma appears less likely due to the low initial Sr–Nd isotopic ratios of the hybrid granitoid rocks. The most felsic sample, N85, is characterized by high silica (~72 wt.%), relatively low Mg# (~28) and moderate I_{Sr} (30.06 Ma) of 0.705864, which would be consistent with the melts derived from the lower crust (Table 3 and Supplementary Table 2). According to the isotopic and whole-rock data, the lower crust-derived magma appears more likely to be a more felsic component in the generation of the hybrid plutons. Furthermore, underplating of the mantle-derived magma and its interaction with the lower crust-derived magma is known as the most desirable mechanism for the production of hybrid magmas (e.g. Rudnick et al., 1986). As noted above, it seems probable that underplating magma could provide the necessary heat source for dehydration melting and produce a granitic melt (e.g. Rushmer, 1991; Roberts and Clemens, 1993; Tepper et al., 1993; Wolf and Wyllie, 1994; Rapp and Watson, 1995; Petford and Gallagher, 2001; Topuz et al., 2005; Karslı et al., 2007).

Adakite is characterized by high Sr/Y and $(La/Yb)_{CN}$ ratios, and low Y and Yb_{CN} values (Defant and Drummond, 1990; Defant et al., 2002; Martin et al., 2005). Considering the $(La/Yb)_{CN}$ and Yb_{CN} content, the studied plutons do not show an adakitic signature (Fig. 14B). Patino-Douce (1999) proposed discrimination diagrams based upon the ratios of the element combinations Al_2O_3–FeO–MgO–TiO_2 and CaO–FeO–MgO–TiO_2 to identify the relative contributions of metasedimentary and mafic sources to granitic melts (Fig. 14C). The low $Al_2O_3/(FeO + MgO + TiO_2)$ ratios and high $Al_2O_3 + FeO + MgO + TiO_2$ values, suggests dehydration melting of the mafic lower crust as the origin source for all the samples in the NPC (that plot within or close to the field of 'amphibolite-derived melts'), except for granitic samples which plot on a continuum within the field of 'greywacke-derived melts' (the greywacke composition is the same as basic and intermediate rocks). However, this may have resulted from the residual mineralogy in the source during the melting of the crustal material. In addition, this could be construed as an amphibole-poor residue in the source, as is indicated by the enrichment of the LREEs.

Additionally, isotopic compositions of the Oligocene NPC indicate a mixing process evidenced by the existence of a linear trend in Fig. 12. The most likely scenario is that the magma derived from the dehydration melting of the lower crust is not the only source for the genesis of the plutons. Furthermore, the underplating mechanism could result in granitic melt by the dehydration melting of the lower crust in the central part of the UDMB.

5.5. Magma interaction processes

The hybrid granitoid rocks and MMEs, by virtue of their formation and widespread occurrence, represent an interaction process for their genesis. Key features in all mafic enclaves are the disequilibrium textures of the phenocrysts in the MMEs which is considered evidence of mingling/mixing. The presence of acicular apatite crystals (Fig. 5H) that may be used as an indication of magma mingling, as presented by Piccoli and Candela (2002) and Vernon (1983), and quartz ocelli (Fig. 5B and D) rimmed by early

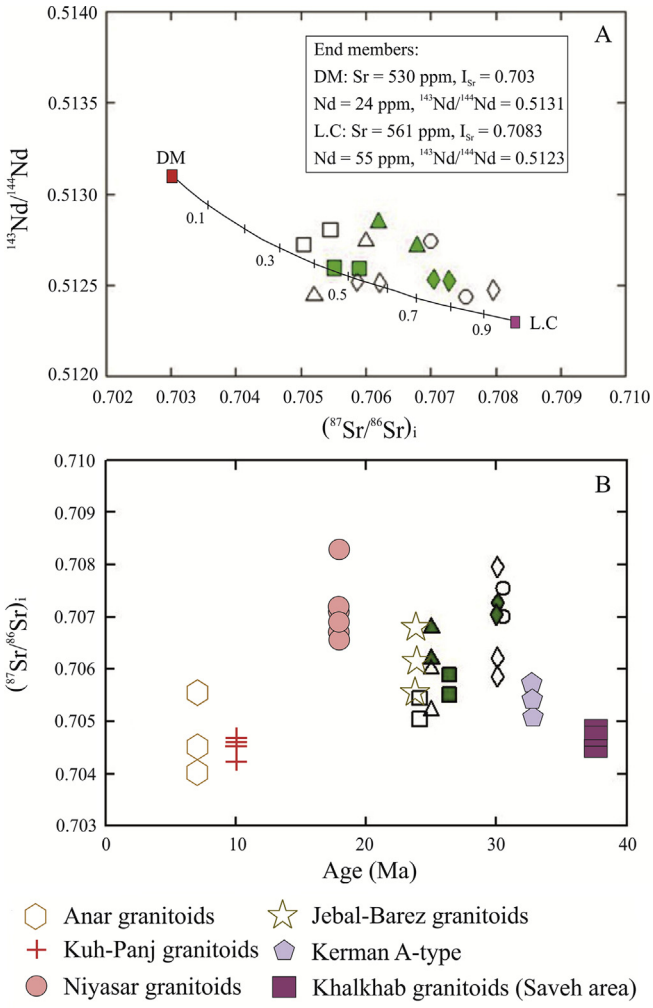

Figure 17. (A) A simple model showing Sr–Nd isotopic variations as a result of magma mixing. (B) Plot of $^{87}Sr/^{86}Sr$ versus age for the NPC samples; Niyasar (Honarmand et al., 2014); Kalkhab (Rezaei-Kahkhaei et al., 2011); Kerman A-type (Dargahi et al., 2010); Anar (Omrani et al., 2008); Jebal-Barez and Kuh-Panj (Shafiei et al., 2009). Symbols are the same as in Fig. 3.

crystallized phases, including fine-grained minerals of the matrix such as hornblende, biotite and plagioclase, suggests disequilibrium textures developed in a new magma (hybrid), and reflect on the hybridization process associated with the generation of the MMEs (Bussy and Ayrton, 1990; Vernon, 1990; Hibbard, 1991, 1995; Janousek et al., 2004). Furthermore, K-feldspar phenocrysts in enclaves (Fig. 5G), do not necessarily connote late or sub-solidus crystallization. Previous experimental studies indicate that abundant liquid is available for crystal growth during K-feldspar nucleation (e.g. Vernon and Paterson, 2008). So, the mechanical transfer of K-feldspar phenocrysts from a more felsic magma into mafic magma has been suggested as a likely process (Vernon, 1990; Hibbard, 1991; Aslan, 2005).

The mixing process is in agreement with the substantial overlap between the data points of the host rocks and their MMEs in the $^{87}Sr/^{86}Sr$ versus $^{143}Nd/^{144}Nd$ ratios plot (Fig. 12B). Moreover, the plots of elemental and oxide compositions against the isotopic variations are ascribed to a magma interaction (e.g. Thirlwall and Jones, 1993; Chen et al., 2002; Chen and Arakawa, 2005; Karslı et al., 2010). The very irregular hyperbolic trend of the samples in the $I_{Sr}(t)$ vs. Sr plot also represents an interaction process in their genesis, although in this diagram, the enclaves display a better hyperbolic trend (Fig. 15). We use two 4-element diagrams to explain the magma interaction process in the genesis of the plutons, as presented by Maia de Hollanda et al. (2003). The defined hyperbolic arrays on Ti/Zr versus Rb/Sr, and the linear trend on Ti/Zr versus Sr/Zr plots display a simple interaction process between at least two separate, distinct compositional end-members (Fig. 16A and B). The binary diagrams of $^{143}Nd/^{144}Nd$ versus $^{147}Sm/^{144}Nd$ and Dy/Yb versus Dy contents shows that the magma interaction process is a credible mechanism along with fractional crystallization in the genesis of these hybrid rocks (Fig. 16C and D). As discussed above, the most likely interpretation for the generation of the NPC rocks is that they represent a mixture of enriched SCLM-derived and lower crust-derived magmas.

A simple mixed model was employed to estimate the relative contribution of mantle and crust components (Fig. 17A). In this model, two-end-members are assumed to represent the average parent magma from the depleted mantle and lower continental crust. Since isotopic ratios of the lower crust component for Iran are unknown, Eastern Pontides values are used instead (Karslı et al., 2010 and references therein). All samples plot on a curve, representing the magma mixing process. Our calculations suggest that ~50% to 90% of lower crust-derived magma and ~10%–50% of the mantle-derived mafic magma were involved in the genesis of the early Oligocene rocks. In contrast, ~45%–65% of the mantle-derived mafic magma may be incorporated with the lower crust-derived magma (~35%–55%) in the generation of the late Oligocene hybrid granitoid rocks. The early Oligocene granitoid rocks contain a higher proportion of crustal material compared to those that formed in the late Oligocene. Petrological and geochemical evidence suggest that at least two distinct magma bodies participated in the genesis of the NPC. Underplating and intrusion of the hot mantle-derived basic magma into the thickened crust could result in dehydration partial melting of the lower continental crust. Widespread interaction between the lower crust-derived magma and mantle-derived melts formed large bodies of hybrid magmas at depths. Eventually, crystal fractionation of these hybrid magmas en route to upper crustal levels generated the various rock types, ranging from diorite to granite, in the central part of the UDMB.

5.6. Comparison with other granitoids in the UDMB

Some subduction-related, mantle-derived granitoids in the UDMB, including Kuh-Panj and Jebal-Barez granitoids, Khalkhab granitoids, Niyasar granitoids and Kerman A-type granitoids, were also plotted for comparison with NPC samples (Fig. 17B). The NPC samples are most similar and consistent with the pre-collisional Eocene–Oligocene Jebal Barez granitoids in the Kerman Cenozoic Magmatic Assemblage (Shafiei et al., 2009). Shafiei et al. (2009) suggested that lower crustal amphibolite melting, together with fractional crystallization and crustal assimilation processes, continue to produce Jebal Barez-type granitoids similar to calc-alkaline magma formed in normal arcs. The melting of a garnet-free basaltic amphibolite source can explain most of the Eocene–Oligocene barren Jebal Barez granodiorites, whereas moderate peridotite melting (5%–20%) and subsequent fractional crystallization of plagioclase and pyroxene best explain the low La/Yb ratios (<10) of the Jebal Barez diorites and quartz diorites. However, in younger adakites, like Anar and Kuh-Panj granitoids, the initial $^{87}Sr/^{86}Sr$ ratios decrease (Fig. 17B), which may be related to late Miocene slab break-off as presented by Omrani et al. (2008).

Nodoushan granitoids and UDMB igneous rocks are isotopically similar. For example, the upper Eocene Kuh-e Dom granitoids from the central UDMB (Sarjoughian et al., 2012) show a high contribution of Cadomian crust (average > 60%). Oligocene lavas

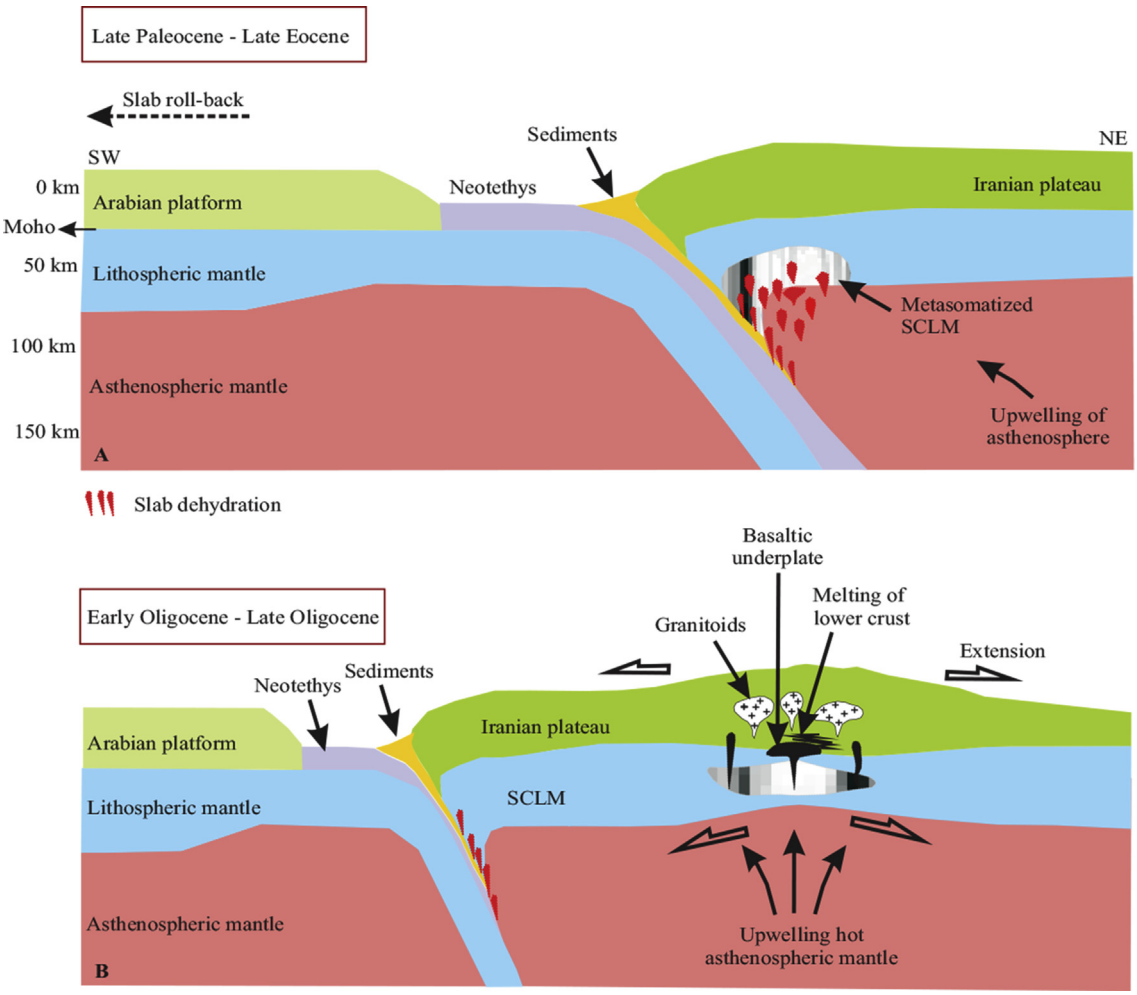

Figure 18. (A–B) Schematic illustration for the geodynamic evolution of the Nodoushan Plutonic Complex. SCLM: Subcontinental lithospheric mantle.

from the Nain area (in the central UDMB) also reflect interaction of mantle melts with upper Cadomian crust (Yeganehfar et al., 2013). The early Eocene to middle Miocene Kashan granitoids (from the central UDMB), show variable isotopic ratios, and Honarmand et al. (2014) concluded that these melts involved ~60%–70% of a lower crust-derived melt and ~30%–40% melt from the SCLM. The Oligo–Miocene (ca. 29 Ma) adakitic and late Eocene shoshonitic (ca. 38 Ma) granitoids from northwestern UDMB may show different sources, resulting from melting of a subducted mélange within the mantle wedge (Aghazadeh et al., 2010) and/or melting of a metasomatized lithospheric mantle (Castro et al., 2013), respectively. The collective age and isotopic data for UDMB igneous rocks and magmatic rocks from the west of Yazd, including the NPC, reveal insignificant differences between the Eocene–Oligocene igneous rocks of Iran. The available information corroborates contributions of continental crust and mantle melts to form UDMB melts.

6. Conclusions and geodynamic implications

According to the unified geochemical, geochronological and Sr–Nd analyses of the host rocks and their MMEs, the following scenario for the NPC from the central part of the UDMB can be outlined. The emplacement of the plutons, which are I-type with metaluminous characteristics and mostly belong to the medium-to-high-K calc-alkaline series, took place at ~30 Ma (middle Rupelian) and ~25 Ma (latest Chattian), as manifested by the U–Pb ages from zircon separates. As has been stated previously, underplating is an acceptable and well-known mechanism for the genesis of hybrid granitoid rocks. Researchers believe that the timing of the underplating is closely related to the major regional tectonic episodes, as well as to the geodynamic processes in deeper parts of the SCLM.

The tectonic evolution and magmatism of the UDMB and the adjoining belt (SSZ) are related to subduction of the Neo-Tethyan oceanic crust beneath the Central Iranian Microcontinent (CIM), and to later collision and post-collision events. Our overall interpretation of Iranian regional geology is that ongoing subduction of the Neo-Tethys beneath Eurasia began as early as the late Triassic and continued until at least the late Oligocene, over some 175 million years (Verdel et al., 2011). Recent studies show that UDMB volcanism was especially widespread from the Eocene to the Oligocene (55–25 Ma; Chiu et al., 2013). It has been proposed that intrusive rocks are dominantly Oligo–Miocene (Berberian and Berberian, 1981). Verdel et al. (2011) concluded that Paleogene magmatism and extension were driven by an episode of slab retreat or slab rollback following a Cretaceous period of flat-slab subduction, analogous to the Laramide and post-Laramide evolution of the western United States. Ghorbani et al. (2014) suggested that the Oligocene–Miocene basic magmatism in the central part of UDMB is compatible with a geodynamic model that includes asthenospheric mantle upwelling prompted by or accompanied by slab

rollback in a subduction-related mantle wedge. Agard et al. (2011) attributed the Oligocene time to a dormant period with strongly reduced or absent magmatic activity.

Eocene extension and lithospheric thinning accompanying slab rollback generated decompression melting of the lithospheric mantle, hydrated by slab-derived fluids and heating from the underlying upwelling asthenosphere (Fig. 18A). The extensional period during the early and late Oligocene probably caused the upwelling of the asthenosphere that triggered the underplating of the mafic magma (Fig. 18B). The thermal anomaly induced by asthenospheric upwelling resulted in partial melting of the chemically-enriched SCLM beneath the Nodoushan area. In fact, in such a case, a hot upwelling asthenosphere is necessary for partial melting of the lithospheric mantle in order to form the parental mafic magma. The subsequent intrusion of the hot, chemically enriched SCLM-derived mafic magma induced the dehydration melting of the lower crust. An extensive interaction between the lower crust-derived melt and SCLM-derived magma, which were chemically enriched in incompatible elements (e.g. Sr, Ba, Rb and LREE) by fluids or melts derived from the dehydration of the old subducting slab and depleted in the isotopic composition, produced the whole spectrum of rock types, ranging from diorite to granite, in the upper crustal levels.

In addition, the Sr-Nd interaction modeling allowed us more accurate identification and even quantification of the two main source components, which are responsible for magma genesis. Modeling based on Sr–Nd isotope data indicates that ~50%–90% of the lower crust-derived melt and ~10%–50% of the mantle-derived mafic magma were involved in the genesis of the early Oligocene magmas. In contrast, ~45%–65% of the mantle-derived mafic magma may be incorporated with the lower crust-derived magma (~35%–55%) in the generation of the late Oligocene hybrid granitoid rocks. As a result, the early Oligocene granitoid rocks contain a higher proportion of crustal material compared to the late Oligocene ones. Nevertheless, the Sr-Nd and geochemical data reveal that some minor contribution from the upper crustal assimilation seems plausible in their generation. The interaction process was followed by fractional crystallization during the rock evolution. The MMEs in the plutons display identical chemical and isotopic composition relative to their host rocks. Considering all data, the MMEs most likely formed by interaction processes between the lower crust-derived felsic and SCLM-derived mafic melts. Interaction processes are proved by very similar isotopic ratios between enclaves and their host rocks, as suggested by Elburg (1996) and Holden et al. (1991). In fact, the MME data supply valuable information with regards to the nature and role of the mantle-derived mafic magmas that were involved in the generation of the hybrid granitoid rocks. These data can also provide insights for the interaction processes between the mantle- and crust-derived magmas.

Acknowledgements

The present study is based on the first author's PhD thesis at Tarbiat Modares University (TMU), Tehran, Iran. Field studies were funded by the TMU Research Grant Council. We are grateful to the Department of Geological Engineering, Middle East Technical University (Ankara, Turkey) and State Key Laboratory of Geological Processes and Mineral Resources, China University of Geosciences (Wuhan), China for kindly helping with geochemistry, isotopic and dating analyses.

Appendix A. Supplementary data

Supplementary data related to this article can be found at https://doi.org/10.1016/j.gsf.2018.03.017.

References

Agard, P., Omrani, J., Jolivet, L., Mouthereau, F., 2005. Convergence history across Zagros (Iran): constraints from collisional and earlier deformation. International Journal of Earth Sciences Geologische Rundschau 94, 401–419. https://doi.org/10.1007/s00531-005-0481-4.

Agard, P., Omrani, J., Jolivet, L., Whitechurch, H., Vrielynck, B., Spakman, W., Monie, P., Meyer, B., Wortel, R., 2011. Zagros orogeny: a subduction-dominated process. Geological Magazine 148, 692–725. https://doi.org/10.1017/S001675681100046X.

Aghazadeh, M., Castro, A., Omran, N.R., Emami, M.H., Moinvaziri, H., Badrzadeh, Z., 2010. The gabbro (shoshonitic)–monzonite–granodiorite association of Khankandi pluton, Alborz Mountains, NW Iran. Journal of Asian Earth Sciences 38, 199–219. https://doi.org/10.1016/j.jseaes.2010.01.002.

Ajaji, T., Weis, D., Giret, A., Bouabdellah, M., 1998. Coeval potassic and sodic calc-alkaline series in the post-collisional Hercynian Tanncherfi intrusive complex, northeastern Morocco: geochemical, isotopic and geochronological evidence. Lithos 45, 371–393. https://doi.org/10.1016/S0024-4937(98)00040-1.

Akal, C., Helvaci, C., 1999. Mafic microgranular enclaves in the Kozak granodiorite, western anatolia. Turkish Journal of Earth Sciences 8, 1–17.

Alavi, M., 2007. Structures of the Zagros fold-thrust belt in Iran. American Journal of Science 307, 1064–1095. https://doi.org/10.2475/09.2007.02.

Alavi, M., 2004. Regional stratigraphy of the Zagros fold-thrust belt of Iran and its proforeland evolution. American Journal of Science 304, 1–20. https://doi.org/10.2475/ajs.304.1.1.

Alavi, M., 1994. Tectonics of the zagros orogenic belt of Iran: new data and interpretations. Tectonophysics 229, 211–238. https://doi.org/10.1016/0040-1951(94)90030-2.

Al-Mishwat, A.T., Nasir, S.J., 2004. Composition of the lower crust of the Arabian Plate: a xenolith perspective. Lithos 72, 45–72. https://doi.org/10.1016/j.lithos.2003.08.003.

Altherr, R., Henjes-Kunst, F., Langer, C., Otto, J., 1999. Interaction between crustal-derived felsic and mantle-derived mafic magmas in the oberkirch pluton (European Variscides, Schwarzwald, Germany). Contributions to Mineralogy and Petrology 137, 304–322. https://doi.org/10.1007/s004100050552.

Amidi, S.M., Emami, M.H., Michel, R., 1984. Alkaline character of Eocene volcanism in the middle part of central Iran and its geodynamic situation. Geologische Rundschau 73, 917–932. https://doi.org/10.1007/BF01820882.

Andersen, T., 2002. Correction of common lead in U–Pb analyses that do not report ^{204}Pb. Chemical Geology 192, 59–79. https://doi.org/10.1016/S0009-2541(02)00195-X.

Aslan, Z., 2005. Petrography and petrology of the calc-alkaline Sarıhan granitoid (NE Turkey): an example of magma mingling and mixing. Turkish Journal of Earth Sciences 14, 185–207.

Ballato, P., Uba, C.E., Landgraf, A., Strecker, M.R., Sudo, M., Stockli, D.F., Friedrich, A., Tabatabaei, S.H., 2011. Arabia-Eurasia continental collision: insights from late Tertiary foreland basin evolution in the Alborz Mountains, northern Iran. Geological Society of America Bulletin 123, 106–131.

Barbarin, B., Didier, J., 1992. Genesis and evolution of mafic microgranular enclaves through various types of interaction between coexisting felsic and mafic magmas. Transactions of the Royal Society of Edinburgh Earth Sciences 83, 145–153. https://doi.org/10.1017/S0263593300007835.

Batchelor, R.A., Bowden, P., 1985. Petrogenetic interpretation of granitoid rock series using multicationic parameters. Chemical Geology 48, 43–55. https://doi.org/10.1016/0009-2541(85)90034-8.

Ben Othman, D., Polve, M., Allègre, C.J., 1984. Nd-Sr isotopic composition of granulites and constraint on the evolution of the lower continental crust. Nature 307, 510–515.

Berberian, F., Berberian, M., 1981. Tectono-plutonic episodes in Iran. In: Gupta, H.K., Delany, F.M. (Eds.), Zagros, Hindu Kush, Himalaya: Geodynamic Evolution. American Geophysical Union, Geodynamics Series, vol. 3, pp. 5–32. https://doi.org/10.1029/GD003p0005.

Berberian, F., Muir, I.D., Pankhurst, R.J., Berberian, M., 1982. Late cretaceous and early Miocene andean-type plutonic activity in northern Makran and Central Iran. Journal of the Geological Society of London 139, 605–614. https://doi.org/10.1144/gsjgs.139.5.0605.

Berberian, M., King, G.C.P., 1981. Towards a paleogeography and tectonic evolution of Iran. Canadian Journal of Earth Sciences 18, 210–265. https://doi.org/10.1139/e81-019.

Bussy, F., Ayrton, S., 1990. Quartz textures in dioritic rocks of hybrid origin. Schweizerische mineralogische und petrographische Mitteilungen 70, 223–235.

Castro, A., Aghazadeh, M., Badrzadeh, Z., Chichorro, M., 2013. Late Eocene–Oligocene post-collisional monzonitic intrusions from the Alborz magmatic belt, NW Iran. An example of monzonite magma generation from a metasomatized mantle source. Lithos 180–181, 109–127. https://doi.org/10.1016/j.lithos.2013.08.003.

Castro, A., Moreno-Ventas, I., de la Rosa, J.D., 1990. Microgranular enclaves as indicators of hybridization processes in granitoid rocks, Hercynian Belt, Spain. Geological Journal 25, 391–404. https://doi.org/10.1002/gj.3350250321.

Chappell, B.W., 1999. Aluminium saturation in I- and S-type granites and the characterization of fractionated haplogranites. Lithos 46, 535–551. https://doi.org/10.1016/S0024-4937(98)00086-3.

Chappell, B.W., White, A.J.R., 1992. I- and S-type granites in the lachlan fold belt. Transactions of the Royal Society of Edinburgh Earth Sciences 83, 1–26. https://doi.org/10.1017/S0263593300007720.

Chappell, B.W., White, A.J.R., 1991. Restite enclaves and the restite model. In: Didier, J., Barbarin, B. (Eds.), Enclaves and Granite Petrology. Elsevier, Amsterdam, pp. 375–381.
Chen, B., Arakawa, Y., 2005. Elemental and Nd-Sr isotopic geochemistry of granitoids from the West Junggar foldbelt (NW China), with implications for Phanerozoic continental growth. Geochimica et Cosmochimica Acta 69, 1307–1320. https://doi.org/10.1016/j.gca.2004.09.019.
Chen, B., Jahn, B.M., Wei, C., 2002. Petrogenesis of Mesozoic granitoids in the Dabie UHP complex, Central China: trace element and Nd–Sr isotope evidence. Lithos 60, 67–88. https://doi.org/10.1016/S0024-4937(01)00077-9.
Chiu, H.-Y., Chung, S.-L., Zarrinkoub, M.H., Mohammadi, S.S., Khatib, M.M., Iizuka, Y., 2013. Zircon U–Pb age constraints from Iran on the magmatic evolution related to Neotethyan subduction and Zagros orogeny. Lithos 162–163, 70–87. https://doi.org/10.1016/j.lithos.2013.01.006.
Collins, W.J., 1998. Evaluation of petrogenetic models for Lachlan Fold Belt granitoids: implications for crustal architecture and tectonic models. Australian Journal of Earth Sciences 45, 483–500. https://doi.org/10.1080/08120099808728406.
Corfu, F., 2004. U-Pb age, setting and tectonic significance of the anorthosite-mangerite-charnockite-granite suite, lofoten-Vesteralen, Norway. Journal of Petrology 45, 1799–1819. https://doi.org/10.1093/petrology/egh034.
Dargahi, S., Arvin, M., Pan, Y., Babaei, A., 2010. Petrogenesis of post-collisional a-type granitoids from the Urumieh–Dokhtar magmatic assemblage, southwestern Kerman, Iran: constraints on the Arabian–Eurasian continental collision. Lithos 115, 190–204. https://doi.org/10.1016/j.lithos.2009.12.002.
De la Roche, H., Leterrier, J., Grandclaude, P., Marchal, M., 1980. A classification of volcanic and plutonic rocks using R1R2-diagram and major-element analyses — its relationships with current nomenclature. Chemical Geology 29, 183–210. https://doi.org/10.1016/0009-2541(80)90020-0.
Defant, M.J., Drummond, M.S., 1990. Derivation of some modern arc magmas by melting of young subducted lithosphere. Nature 347, 662–665. https://doi.org/10.1038/347662a0.
Defant, M.J., Kepezhinskas, P., Xu, J.F., Wang, Q., Zhang, Q., Xiao, L., 2002. Adakites: some variations on a theme. Acta Petrologica Sinica 18, 129–142.
Dias, G., Leterrier, J., 1994. The genesis of felsic-mafic plutonic associations: a Sr and Nd isotopic study of the Hercynian Braga Granitoid Massif (Northern Portugal). Lithos 32, 207–223. https://doi.org/10.1016/0024-4937(94)90040-X.
Didier, J., 1984. The problem of enclaves in granitic rocks, a review of recent ideas on their origin. In: Xu, K.Q., Tu, G.C. (Eds.), Geology of Granite and Their Metallogenetic Relations. Proceedings International Symposium, Nanjing, October 1982. Science Press, Beijing, pp. 137–144.
Didier, J., 1973. Granites and Their Enclaves. Elsevier, Amsterdam, p. 393.
Didier, J., Barbarin, B., 1991. The different types of enclaves in granites-nomenclature. In: Didier, J., Barbarin, B. (Eds.), Enclaves and Granite Petrology. Elsevier, Amsterdam, pp. 19–24.
Donaire, T., Pascual, E., Pin, C., Duthou, J.-L., 2005. Microgranular enclaves as evidence of rapid cooling in granitoid rocks: the case of the Los Pedroches granodiorite, Iberian Massif, Spain. Contributions to Mineralogy and Petrology 149, 247–265. https://doi.org/10.1007/s00410-005-0652-0.
Dorais, M.J., Whitney, J.A., Roden, M.F., 1990. Origin of mafic enclaves in the Dinkey creek pluton, central Sierra Nevada batholith, California. Journal of Petrology 31, 853–881. https://doi.org/10.1093/petrology/31.4.853.
Elburg, M.A., 1996. Evidence of isotopic equilibration between microgranitoid enclaves and host granodiorite, Warburton Granodiorite, Lachlan Fold Belt, Australia. Lithos 38, 1–22. https://doi.org/10.1016/0024-4937(96)00003-5.
Ellouz-Zimmermann, N., Lallemant, S.J., Castilla, R., Mouchot, N., Leturmy, P., Battani, A., Buret, C., Cherel, L., Desaubliaux, G., Deville, E., Ferrand, J., Lügcke, A., Mahieux, G., Mascle, G., Mühr, P., Pierson-Wickmann, A.-C., Robion, P., Schmitz, J., Danish, M., Hasany, S., Shahzad, A., Tabreez, A., 2007. Offshore frontal part of the Makran accretionary prism: the Chamak Survey (Pakistan). In: Lacombe, O., Roure, F., Lavé, J., Vergés, J. (Eds.), Thrust Belts and Foreland Basins:from Fold Kinematics to Hydrocarbon Systems. Frontiers in Earth Sciences. Springer, Berlin, Heidelberg, pp. 351–366. https://doi.org/10.1007/978-3-540-69426-7_18.
Ferré, E.C., Leake, B.E., 2001. Geodynamic significance of early orogenic high-K crustal and mantle melts: example of the Corsica Batholith. Lithos 59, 47–67. https://doi.org/10.1016/S0024-4937(01)00060-3.
Frost, T.P., Mahood, G.A., 1987. Field, chemical, and physical constraints on mafic-felsic magma interaction in the Lamarck Granodiorite, Sierra Nevada, California. Geological Society of America Bulletin 99, 272–291. https://doi.org/10.1130/0016-7606(1987)99<272:FCAPCO>2.0.CO;2.
Gao, Y., Hou, Z., Kamber, B.S., Wei, R., Meng, X., Zhao, R., 2007. Adakite-like porphyries from the southern Tibetan continental collision zones: evidence for slab melt metasomatism. Contributions to Mineralogy and Petrology 153, 105–120. https://doi.org/10.1007/s00410-006-0137-9.
Ghalamghash, J., Mohammadiha, K., 2005. Geological map of Kafeh-e-Taghestan: Iran. Geological Survey of Iran scale 1, 100,000 Sheet.
Ghorbani, M.R., Graham, I.T., Ghaderi, M., 2014. Oligocene–Miocene geodynamic evolution of the central part of Urumieh-Dokhtar Arc of Iran. International Geology Review 56, 1039–1050. https://doi.org/10.1080/00206814.2014.919615.
Grove, T.L., Donnelly-Nolan, J.M., 1986. The evolution of young silicic lavas at Medicine Lake Volcano, California: implications for the origin of compositional gaps in calc-alkaline series lavas. Contributions to Mineralogy and Petrology 92, 281–302. https://doi.org/10.1007/BF00572157.
Han, B.F., Wang, S.G., Jahn, B.M., Hong, D.W., Kagami, H., Sun, Y.L., 1997. Depleted-mantle source for the Ulungur River A-type granites from North Xinjiang, China: geochemistry and Nd–Sr isotopic evidence, and implications for Phanerozoic crustal growth. Chemical Geology 138, 135–159. https://doi.org/10.1016/S0009-2541(97)00003-X.
Hassanzadeh, J., Stockli, D.F., Horton, B.K., Axen, G.J., Stockli, L.D., Grove, M., Schmitt, A.K., Walker, J.D., 2008. U-Pb zircon geochronology of late Neoproterozoic–Early Cambrian granitoids in Iran: implications for paleogeography, magmatism, and exhumation history of Iranian basement. Tectonophysics 451, 71–96. https://doi.org/10.1016/j.tecto.2007.11.062.
Hawkesworth, C.J., Gallagher, K., Hergt, J.M., McDermott, F., 1993. Mantle and slab contributions in arcmagmas. Annual Review of Earth and Planetary Sciences 21, 175–204. https://doi.org/10.1146/annurev.ea.21.050193.001135.
Hibbard, M.J., 1995. Petrography to Petrogenesis. Prentice Hall, New Jersey.
Hibbard, M.J., 1991. Textural anatomy of twelve magma-mixed granitoid systems. In: Didier, J., Barbarin, B. (Eds.), Enclaves and Granite Petrology. Elsevier, Amsterdam, pp. 431–444.
Hine, R., Williams, I.S., Chappell, B.W., White, A.J.R., 1978. Contrasts between I - and S -type granitoids of the Kosciusko batholith. Journal of the Geological Society of Australia 25, 219–234. https://doi.org/10.1080/00167617808729029.
Holden, P., Halliday, A.N., Stephens, W.E., Henney, P.J., 1991. Chemical and isotopic evidence for major mass transfer between mafic enclaves and felsic magma. Chemical Geology 92, 135–152. https://doi.org/10.1016/0009-2541(91)90053-T.
Holden, P., Halliday, A.N., Stephens, W.E., 1987. Neodymium and strontium isotope content of microdiorite enclaves points to mantle input to granitoid production. Nature 330, 53–56. https://doi.org/10.1038/330053a0.
Holten, T., Jamtveit, B., Meakin, P., 2000. Noise and oscillatory zoning of minerals. Geochimica et Cosmochimica Acta 64, 1893–1904. https://doi.org/10.1016/S0016-7037(99)00444-5.
Honarmand, M., Rashidnejad Omran, N., Corfu, F., Emami, M.H., Nabatian, G., 2013. Geochronology and magmatic history of a calc-alkaline plutonic complex in the Urumieh–Dokhtar Magmatic Belt, Central Iran: zircon ages as evidence for two major plutonic episodes. Journal of Mineralogy and Geochemistry 190, 67–77. https://doi.org/10.1127/0077-7757/2013/0230.
Honarmand, M., Rashidnejad Omran, N., Neubauer, F., Hashem Emami, M., Nabatian, G., Liu, X., Dong, Y., von Quadt, A., Chen, B., 2014. Laser-ICP-MS U–Pb zircon ages and geochemical and Sr–Nd–Pb isotopic compositions of the Niyasar plutonic complex, Iran: constraints on petrogenesis and tectonic evolution. International Geology Review 56, 104–132. https://doi.org/10.1080/00206814.2013.820375.
Hou, Z., Zhang, H., Pan, X., Yang, Z., 2011. Porphyry Cu (–Mo–Au) deposits related to melting of thickened mafic lower crust: examples from the eastern Tethyan metallogenic domain. Ore Geology Reviews 39, 21–45. https://doi.org/10.1016/j.oregeorev.2010.09.002.
Huppert, H.E., Sparks, R.S.J., 1988. The generation of granitic magmas by intrusion of basalt into continental crust. Journal of Petrology 29, 599–624. https://doi.org/10.1093/petrology/29.3.599.
Jaffey, A.H., Flynn, K.F., Glendenin, L.E., Bentley, W.C., Essling, A.M., 1971. Precision measurement of half-lives and specific activities of ^{235}U and ^{238}U. Physical Review C 4, 1889–1906. https://doi.org/10.1103/PhysRevC.4.1889.
Janousek, V., Braithwaite, C.J.R., Bowes, D.R., Gerdes, A., 2004. Magma-mixing in the genesis of Hercynian calc-alkaline granitoids: an integrated petrographic and geochemical study of the Sázava intrusion, Central Bohemian Pluton, Czech Republic. Lithos 78, 67–99. https://doi.org/10.1016/j.lithos.2004.04.046.
Karslı, O., Chen, B., Aydin, F., Şen, C., 2007. Geochemical and Sr–Nd–Pb isotopic compositions of the Eocene Dölek and Sariçiçek Plutons, Eastern Turkey: implications for magma interaction in the genesis of high-K calc-alkaline granitoids in a post-collision extensional setting. Lithos 98, 67–96. https://doi.org/10.1016/j.lithos.2007.03.005.
Karslı, O., Dokuz, A., Uysal, İ., Aydin, F., Chen, B., Kandemir, R., Wijbrans, J., 2010. Relative contributions of crust and mantle to generation of Campanian high-K calc-alkaline I-type granitoids in a subduction setting, with special reference to the Harşit Pluton, Eastern Turkey. Contributions to Mineralogy and Petrology 160, 467–487. https://doi.org/10.1007/s00410-010-0489-z.
Kay, S.M., Mpodozis, C., 2001. Central Andean ore deposits linked to evolving shallow subduction systems and thickening Crust. GSA Today Geological Society of America 11, 4–9.
Kim, J.S., Shin, K.C., Lee, J.D., 2002. Petrographical study on the Yucheon granite and its enclaves. Geosciences Journal 6, 289–302. https://doi.org/10.1007/BF03020614.
Köksal, S., Göncüoğlu, M.C., 2008. Sr and Nd isotopic characteristics of some S-, I- and a-type granitoids from central anatolia. Turkish Journal of Earth Sciences 17, 111–127.
Köksal, S., Toksoy-Köksal, F., Göncüoğlu, M.C., 2017. Petrogenesis and geodynamics of plagiogranites from Central Turkey (Ekecikdağ/Aksaray): new geochemical and isotopic data for generation in an arc basin system within the northern branch of Neotethys. International Journal of Earth Sciences 106 (4), 1181–1203. https://doi.org/10.1007/s00531-016-1401-5.
Krogh, T.E., 1973. A low-contamination method for hydrothermal decomposition of zircon and extraction of U and Pb for isotopic age determinations. Geochimica et Cosmochimica Acta 37, 485–494. https://doi.org/10.1016/0016-7037(73)90213-5.

Kumar, S., Rino, V., Pal, A.B., 2004. Field evidence of magma mixing from microgranular enclaves hosted in palaeoproterozoic malanjkhand granitoids, Central India. Gondwana Research 7, 539–548. https://doi.org/10.1016/S1342-937X(05)70804-2.

Lameyre, J., Bowden, P., 1982. Plutonic rock type series: discrimination of various granitoid series and related rocks. Journal of Volcanology and Geothermal Research 14, 169–186.

Link, A.J., 1969. Inclusions of the Half Dome Quartz Monzonite, Yosemite National Park, California (PhD Thesis). (Geology)-Northwestern University, Illinois, USA.

Liu, Y., Gao, S., Hu, Z., Gao, C., Zong, K., Wang, D., 2010. Continental and oceanic crust recycling-induced melt-peridotite interactions in the Trans-North China Orogen: U-Pb dating, Hf isotopes and trace elements in zircons from mantle xenoliths. Journal of Petrology 51, 537–571. https://doi.org/10.1093/petrology/egp082.

Liu, Y., Hu, Z., Gao, S., Günther, D., Xu, J., Gao, C., Chen, H., 2008. In situ analysis of major and trace elements of anhydrous minerals by LA-ICP-MS without applying an internal standard. Chemical Geology 257, 34–43. https://doi.org/10.1016/j.chemgeo.2008.08.004.

López, S., Castro, A., 2001. Determination of the fluid–absent solidus and supersolidus phase relationships of MORB-derived amphibolites in the range 4–14 kbar. American Mineralogist 86, 1396–1403. https://doi.org/10.2138/am-2001-11-1208.

Ludwig, K.R., 2003. Isoplot 3: a geochronological toolkit for microsoft excel. Berkeley Geochronology Centre Special Publication 4, 74.

Ludwig, K.R., 1999. Isoplot/ex version 2.03. A geochronological toolkit for Microsoft Excel. Berkely Geochronology under Special Publication 1, 43.

Maia de Hollanda, M.H.B., Pimentel, M.M., Jardim de Sá, E.F., 2003. Paleoproterozoic subduction-related metasomatic signatures in the lithospheric mantle beneath NE Brazil: inferences from trace element and Sr–Nd–Pb isotopic compositions of Neoproterozoic high-K igneous rocks. Journal of South American Earth Sciences 15, 885–900. https://doi.org/10.1016/S0895-9811(03)00014-2.

Maniar, P.D., Piccoli, P.M., 1989. Tectonic discrimination of granitoids. Geological Society of America Bulletin 101, 635–643. https://doi.org/10.1130/0016-7606(1989)101<0635:TDOG>2.3.CO;2.

Martin, H., Smithies, R.H., Rapp, R., Moyen, J.-F., Champion, D., 2005. An overview of adakite, tonalite–trondhjemite–granodiorite (TTG), and sanukitoid: relationships and some implications for crustal evolution. Lithos 79, 1–24. https://doi.org/10.1016/j.lithos.2004.04.048.

Mattinson, J.M., 2005. Zircon U–Pb chemical abrasion ("CA-TIMS") method: combined annealing and multi-step partial dissolution analysis for improved precision and accuracy of zircon ages. Chemical Geology 220, 47–66. https://doi.org/10.1016/j.chemgeo.2005.03.011.

Mohajjel, M., Fergusson, C.L., 2014. Jurassic to cenozoic tectonics of the zagros orogen in northwestern Iran. International Geology Review 56, 263–287. https://doi.org/10.1080/00206814.2013.853919.

Mohajjel, M., Fergusson, C.L., Sahandi, M.R., 2003. Cretaceous–tertiary convergence and continental collision, Sanandaj–Sirjan zone, western Iran. Journal of Asian Earth Sciences 21, 397–412. https://doi.org/10.1016/S1367-9120(02)00035-4.

Moore, J.G., Sisson, T.W., 2008. Igneous phenocrystic origin of K-feldspar megacrysts in granitic rocks from the Sierra Nevada batholith. Geosphere 4, 387–400. https://doi.org/10.1130/GES00146.1.

Nakamura, N., 1974. Determination of REE, Ba, Fe, Mg, Na and K in carbonaceous and ordinary chondrites. Geochimica et Cosmochimica Acta 38, 757–775. https://doi.org/10.1016/0016-7037(74)90149-5.

Nittmann, J., Daccord, G., Stanley, H.E., 1985. Fractal growth viscous fingers: quantitative characterization of a fluid instability phenomenon. Nature 314, 141–144. https://doi.org/10.1038/314141a0.

Omrani, J., Agard, P., Whitechurch, H., Benoit, M., Prouteau, G., Jolivet, L., 2008. Arc-magmatism and subduction history beneath the Zagros Mountains, Iran: a new report of adakites and geodynamic consequences. Lithos 106, 380–398. https://doi.org/10.1016/j.lithos.2008.09.008.

Parada, M.A., Nystrom, J.O., Levi, B., 1999. Multiple sources for the Coastal Batholith of central Chile (31-34°S): geochemical and Sr-Nd isotopic evidence and tectonic implications. Lithos 46, 505–521.

Paterson, S.R., Pignotta, G.S., Vernon, R.H., 2004. The significance of microgranitoid enclave shapes and orientations. Journal of Structural Geology 26, 1465–1481. https://doi.org/10.1016/j.jsg.2003.08.013.

Patino-Douce, A.E., 1999. What do experiments tell us about the relative contributions of crust and mantle to the origin of granitic magmas?. In: Castro, A., Fernandez, C., Vigneresse, J.L. (Eds.), Understanding Granites: Integrating New and Classical Techniques. Geological Society, London, Special Publications, vol. 168, pp. 55–75. https://doi.org/10.1144/GSL.SP.1999.168.01.05.

Pearce, J.A., Harris, N.B.W., Tindle, A.G., 1984. Trace element discrimination diagrams for the tectonic interpretation of granitic rocks. Journal of Petrology 25, 956–983. https://doi.org/10.1093/petrology/25.4.956.

Peccerillo, A., Taylor, S.R., 1976. Geochemistry of Eocene calc-alkaline volcanic rocks from the Kastamonu area, Northern Turkey. Contributions to Mineralogy and Petrology 58, 63–81. https://doi.org/10.1007/BF00384745.

Perugini, D., Poli, G., 2000. Chaotic dynamics and fractals in magmatic interaction processes: a different approach to the interpretation of mafic microgranular enclaves. Earth and Planetary Science Letters 175, 93–103. https://doi.org/10.1016/S0012-821X(99)00282-4.

Perugini, D., Poli, G., Christofides, G., Eleftheriadis, G., 2003. Magma mixing in the Sithonia Plutonic Complex, Greece: evidence from mafic microgranular enclaves. Mineralogy and Petrology 78, 173–200. https://doi.org/10.1007/s00710-002-0225-0.

Perugini, D., Ventura, G., Petrelli, M., Poli, G., 2004. Kinematic significance of morphological structures generated by mixing of magmas: a case study from Salina Island (southern Italy). Earth and Planetary Science Letters 222, 1051–1066. https://doi.org/10.1016/j.epsl.2004.03.038.

Petford, N., Gallagher, K., 2001. Partial melting of mafic (amphibolitic) lower crust by periodic influx of basaltic magma. Earth and Planetary Science Letters 193, 483–499. https://doi.org/10.1016/S0012-821X(01)00481-2.

Piccoli, P.M., Candela, P.A., 2002. Apatite in igneous systems. Reviews in Mineralogy and Geochemistry 48, 255–292. https://doi.org/10.2138/rmg.2002.48.6.

Pin, C., Binon, M., Belin, J.M., Barbarin, B., Clemens, J.D., 1990. Origin of microgranular enclaves in granitoids: equivocal Sr-Nd evidence from Hercynian rocks in the massif central (France). Journal of Geophysical Research Solid Earth 95, 17821–17828. https://doi.org/10.1029/JB095iB11p17821.

Poli, G.E., Tommasini, S., 1991. Model for the origin and significance of microgranular enclaves in calc-alkaline granitoids. Journal of Petrology 32, 657–666. https://doi.org/10.1093/petrology/32.3.657.

Ramezani, J., Tucker, R.D., 2003. The Saghand region, Central Iran: U-Pb geochronology, petrogenesis and implications for Gondwana tectonics. American Journal of Science 303, 622–665. https://doi.org/10.2475/ajs.303.7.622.

Rapp, R.P., Watson, E.B., 1995. Dehydration melting of metabasalt at 8-32 kbar: implications for continental growth and crust-mantle recycling. Journal of Petrology 36, 891–931. https://doi.org/10.1093/petrology/36.4.891.

Rapp, R.P., Watson, E.B., Miller, C.F., 1991. Partial melting of amphibolite/eclogite and the origin of Archean trondhjemites and tonalites. Precambrian Research 51, 1–25. https://doi.org/10.1016/0301-9268(91)90092-O.

Rezaei-Kahkhaei, M., Galindo, C., Pankhurst, R.J., Esmaeily, D., 2011. Magmatic differentiation in the calc-alkaline Khalkhab–Neshveh pluton, Central Iran. Journal of Asian Earth Sciences 42, 499–514. https://doi.org/10.1016/j.jseaes.2011.04.022.

Richards, J.P., Boyce, A.J., Pringle, M.S., 2001. Geologic evolution of the Escondida area, northern Chile: amodel for spatial and temporal localization of porphyry Cu mineralization. Economic Geology 96, 271–305. https://doi.org/10.2113/gsecongeo.96.2.271.

Roberts, M.P., Clemens, J.D., 1993. Origin of high-potassium, talc-alkaline, I-type granitoids. Geology 21, 825–828. https://doi.org/10.1130/0091-7613(1993)021<0825:OOHPTA>2.3.CO;2.

Rollinson, H.R., 1993. Using Geochemical Data: Evaluation, Presentation, Interpretation. Longman Scientific and Technical, London, p. 352.

Rottura, A., Bargossi, G.M., Caggianelli, A., Del Moro, A., Visona, D., Tranne, C.A., 1998. Origin and significance of the Permian high-K calc-alkaline magmatism in the central-eastern Southern Alps, Italy. Lithos 45, 329–348. https://doi.org/10.1016/S0024-4937(98)00038-3.

Rudnick, R.L., McDonough, W.F., McCulloch, M.T., Taylor, S.R., 1986. Lower crustal xenoliths from Queensland, Australia: evidence for deep crustal assimilation and fractionation of continental basalts. Geochimica et Cosmochimica Acta 50, 1099–1115. https://doi.org/10.1016/0016-7037(86)90391-1.

Rushmer, T., 1991. Partial melting of two amphibolites: contrasting experimental results under fluid-absent conditions. Contributions to Mineralogy and Petrology 107, 41–59. https://doi.org/10.1007/BF00311184.

Sarjoughian, F., Kananian, A., Haschke, M., Ahmadian, J., Ling, W., Zong, K., 2012. Magma mingling and hybridization in the Kuh-e Dom pluton, Central Iran. Journal of Asian Earth Sciences 54–55, 49–63. https://doi.org/10.1016/j.jseaes.2012.03.013.

Schandl, E.S., Gorton, M.P., 2002. Application of high field strength elements to discriminate tectonic settings in VMS environments. Economic Geology 97, 629–642. https://doi.org/10.2113/97.3.629.

Scharer, U., 1984. The effect of initial ^{230}Th disequilibrium on young UPb ages: the Makalu case, Himalaya. Earth and Planetary Science Letters 67, 191–204. https://doi.org/10.1016/0012-821X(84)90114-6.

Şen, C., Dunn, T., 1994. Dehydration melting of a basaltic composition amphibolite at 1.5 and 2.0 GPa: implications for the origin of adakites. Contributions to Mineralogy and Petrology 117, 394–409. https://doi.org/10.1007/BF00307273.

Şen, P.A., Temel, A., Gourgaud, A., 2004. Petrogenetic modelling of Quaternary post-collisional volcanism: a case study of central and eastern Anatolia. Geological Magazine 141, 81–98. https://doi.org/10.1017/S0016756803008550.

Shafiei, B., Haschke, M., Shahabpour, J., 2009. Recycling of orogenic arc crust triggers porphyry Cu mineralization in Kerman Cenozoic arc rocks, southeastern Iran. Mineralium Deposita 44, 265–283. https://doi.org/10.1007/s00126-008-0216-0.

Shahabpour, J., 2007. Island-arc affinity of the central Iranian volcanic belt. Journal of Asian Earth Sciences 30, 652–665. https://doi.org/10.1016/j.jseaes.2007.02.004.

Shahsavari Alavijeh, B., Rashidnejad-Omran, N., Corfu, F., 2017. Zircon U-Pb ages and emplacement history of the Nodoushan plutonic complex in the central Urumieh-Dokhtar magmatic belt, Central Iran: product of Neotethyan subduction during the Paleogene. Journal of Asian Earth Sciences 143, 283–295. https://doi.org/10.1016/j.jseaes.2017.03.034.

Smit, J., Burg, J.-P., Dolati, A., Sokoutis, D., 2010. Effects of mass waste events on thrust wedges: analogue experiments and application to the Makran accretionary wedge. Tectonics 29. https://doi.org/10.1029/2009TC002526. TC3003–11.

Soesoo, A., 2000. Fractional crystallization of mantle-derived melts as a mechanism for some I-type granite petrogenesis: an example from Lachlan Fold Belt,

Australia. Journal of the Geological Society 157, 135–149. https://doi.org/10.1144/jgs.157.1.135.
Stacey, J.S., Kramers, J.D., 1975. Approximation of terrestrial lead isotope evolution by a two-stage model. Earth and Planetary Science Letters 26, 207–221. https://doi.org/10.1016/0012-821X(75)90088-6.
Streckeisen, A.L., 1976. To each plutonic rock its proper name. Earth Science Reviews 12, 1–33.
Sun, S.S., McDonough, W.F., 1989. Chemical and isotopic systematics of oceanic basalts: implications for mantle composition and processes. In: Saunders, A.D., Norry, M.J. (Eds.), Magmatism in Ocean Basins. Geological Society of London, vol. 42. Special Publication, pp. 313–345. https://doi.org/10.1144/GSL.SP.1989.042.01.19.
Taylor, S.R., McLennan, S.M., 1985. The Continental Crust: its Composition and Evolution. Blackwell Sci. Pub, Blackwell, Oxford, UK, p. 312.
Tepper, J.H., Nelson, B.K., Bergantz, G.W., Irving, A.J., 1993. Petrology of the Chilliwack batholith, North Cascades, Washington: generation of calc-alkaline granitoids by melting of mafic lower crust with variable water fugacity. Contributions to Mineralogy and Petrology 113, 333–351. https://doi.org/10.1007/BF00286926.
Thirlwall, M.F., Jones, N.W., 1993. Isotope geochemistry and contamination mechanism of Tertiary lavas from Skye, northwest Scotland. In: Hawkesworth, C.J., Norry, M.J. (Eds.), Continental Basalts and Mantle Xenoliths. Shiva, Cheshire, pp. 186–208.
Topuz, G., Altherr, R., Schwarz, W.H., Siebel, W., Satır, M., Dokuz, A., 2005. Post-collisional plutonism with adakite-like signatures: the Eocene Saraycık granodiorite (eastern Pontides, Turkey). Contributions to Mineralogy and Petrology 150, 441–455. https://doi.org/10.1007/s00410-005-0022-y.
Turner, S.P., Foden, J.D., Morrison, R.S., 1992. Derivation of some A-type magmas by fractionation of basaltic magma: an example from the Padthaway Ridge, South Australia. Lithos 28, 151–179. https://doi.org/10.1016/0024-4937(92)90029-X.
Verdel, C., Wernicke, B.P., Hassanzadeh, J., Guest, B., 2011. A Paleogene extensional arc flare-up in Iran. Tectonics 30, 1–20. https://doi.org/10.1029/2010TC002809.
Vernon, R.H., 1991. Interpretation of microstructures of microgranitoid enclaves. In: Didier, J., Barbarin, B. (Eds.), Enclaves and Granite Petrology. Elsevier, Amsterdam, pp. 277–291.
Vernon, R.H., 1990. Crystallization and hybridism in microgranitoid enclave magmas: microstructural evidence. Journal of Geophysical Research 95, 17849–17859. https://doi.org/10.1029/JB095iB11p17849.
Vernon, R.H., 1984. Microgranitoid enclaves in granites-globules of hybrid magma quenched in a plutonic environment. Nature 309, 438–439. https://doi.org/10.1038/309438a0.
Vernon, R.H., 1983. Restite, xenoliths and microgranitoid enclaves in granites. Journal and Proceedings of the Royal Society of New South Wales 116, 77–103.
Vernon, R.H., Paterson, S.R., 2008. How late are K-feldspar megacrysts in granites? Lithos 104, 327–336. https://doi.org/10.1016/j.lithos.2008.01.001.
Volkert, R.A., Feigenson, M.D., Patino, L.C., Delaney, J.S., Drake Jr., A.A., 2000. Sr and Nd isotopic compositions, age and petrogenesis of A-type granitoids of the Vernon Supersuite, New Jersey Highlands, USA. Lithos 50, 325–347. https://doi.org/10.1016/S0024-4937(99)00065-1.
Waight, T.E., Maas, R., Nicholls, I.A., 2000. Fingerprinting feldspar phenocrysts using crystal isotopic composition stratigraphy: implications for crystal transfer and magma mingling in S-type granites. Contributions to Mineralogy and Petrology 139, 227–239. https://doi.org/10.1007/s004100000128.
Weinberg, R.F., Sial, A.N., Pessoa, R.R., 2001. Magma flow within the Tavares pluton, northeastern Brazil: compositional and thermal convection. Geological Society of America Bulletin 113, 508–520.
White, A.J.R., Chappell, B.W., Wyborn, D., 1999. Application of the restite model to the deddick granodiorite and its enclaves -a reinterpretation of the observations and data of Maas et al. (1997). Journal of Petrology 40, 413–421. https://doi.org/10.1093/petroj/40.3.413.
Whitney, D.L., Evans, B.W., 2010. Abbreviations for names of rock-forming minerals. American Mineralogist 95, 185–187. https://doi.org/10.2138/am.2010.3371.
Wiebe, R.A., 1991. Commingling of contrasted magmas and generation of mafic enclaves in granitic rocks. In: Didier, J., Barbarin, B. (Eds.), Enclaves and Granite Petrology. Dev. Petrology, vol. 13, pp. 393–402.
Wiebe, R.A., 1996. Mafic-silicic layered intrusions: the role of basaltic injections on magmatic processes and the evolution of silicic magma chambers. Transactions of the Royal Society of Edinburgh Earth Sciences 87, 233–242. https://doi.org/10.1017/S0263593300006647.
Wiebe, R.A., Smith, D., Sturm, M., King, E.M., Seckler, M.S., 1997. Enclaves in the Cadillac Mountain Granite (Coastal Maine): samples of hybrid magma from the base of the chamber. Journal of Petrology 38, 393–423. https://doi.org/10.1093/petroj/38.3.393.
Wilson, M., 1989. Igneous Petrogenesis. Chapman and Hall, London, p. 466.
Winther, K.T., 1996. An experimentally based model for the origin of tonalitic and trondhjemitic melts. Chemical Geology 127, 43–59. https://doi.org/10.1016/0009-2541(95)00087-9.
Wolf, M.B., Wyllie, P.J., 1994. Dehydration-melting of amphibolite at 10 kbar: the effects of temperature and time. Contributions to Mineralogy and Petrology 115, 369–383. https://doi.org/10.1007/BF00320972.
Wyllie, P.J., Wolf, M.B., 1993. Amphibolite dehydration-melting: sorting out the solidus. In: Prichard, H.M., Alabaster, T., Harris, N.B.W., Neary, C.R. (Eds.), Magmatic Processes and Plate Tectonics. Geological Society, London, Special Publications, vol. 76, pp. 405–416. https://doi.org/10.1144/GSL.SP.1993.076.01.20.
Yeganehfar, H., Ghorbani, M.R., Shinjo, R., Ghaderi, M., 2013. Magmatic and geodynamic evolution of Urumieh–Dokhtar basic volcanism, Central Iran: major, trace element, isotopic, and geochronologic implications. International Geology Review 55, 767–786. https://doi.org/10.1080/00206814.2012.752554.
Yuan, H., Gao, S., Liu, X., Li, H., Günther, D., Wu, F., 2004. Accurate U-Pb age and trace element determinations of zircon by laser ablation-inductively coupled plasma-mass Spectrometry. Geostandards and Geoanalytical Research 28, 353–370. https://doi.org/10.1111/j.1751-908X.2004.tb00755.x.
Zindler, A., Hart, S.R., 1986. Chemical geodynamics. Annual Review of Earth and Planetary Sciences 14, 493–571. https://doi.org/10.1146/annurev.ea.14.050186.002425.